

CHEN, Y., DUAN, W., HE, Y., WANG, S. and FERNANDEZ, C. 2024. A hybrid data driven framework considering feature extraction for battery state of health estimation and remaining useful life prediction. Green energy and intelligent transportation [online], In Press, article number 100160. Available from:
<https://doi.org/10.1016/j.geits.2024.100160>

A hybrid data driven framework considering feature extraction for battery state of health estimation and remaining useful life prediction.

CHEN, Y., DUAN, W., HE, Y. WANG, S. and FERNANDEZ, C.

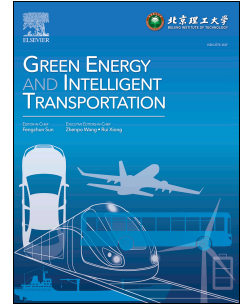
2024

© 2024 Published by Elsevier Ltd on behalf of Beijing Institute of Technology Press Co., Ltd.

Journal Pre-proof

A Hybrid Data Driven Framework Considering Feature Extraction for Battery State of Health Estimation and Remaining Useful Life Prediction

Yuan Chen, Wenxian Duan, Yigang He, Shunli Wang, Carlos Fernandez



PII: S2773-1537(24)00012-4

DOI: <https://doi.org/10.1016/j.geits.2024.100160>

Reference: GEITS 100160

To appear in: *Green Energy and Intelligent Transportation*

Received Date: 2 August 2023

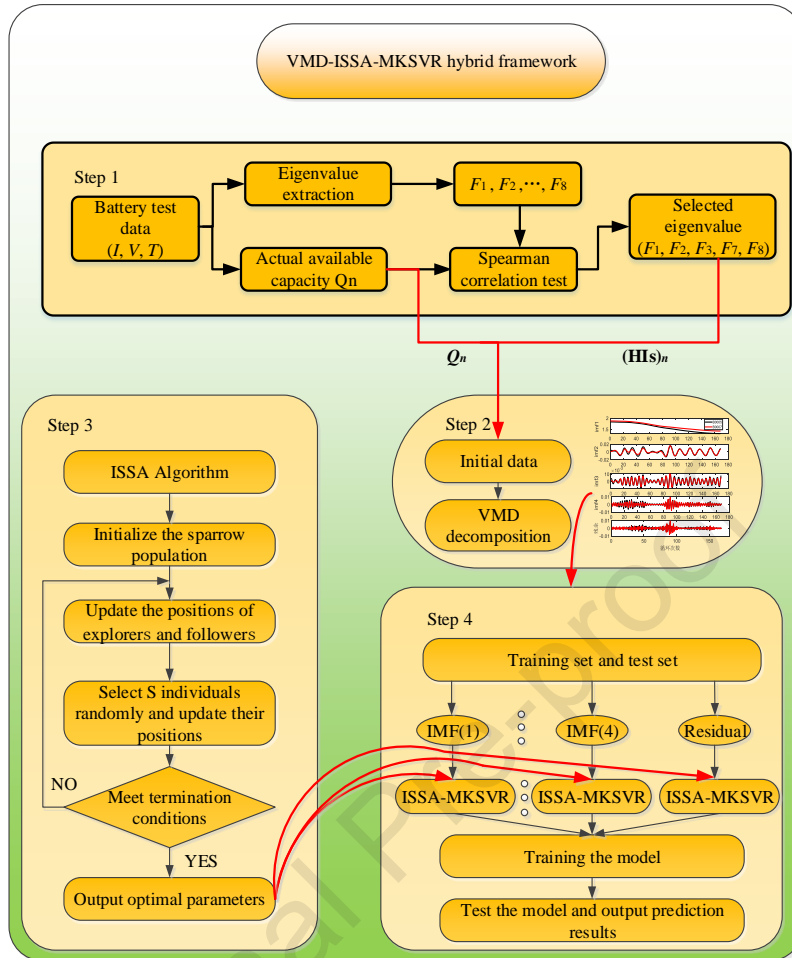
Revised Date: 20 September 2023

Accepted Date: 27 September 2023

Please cite this article as: Chen Y, Duan W, He Y, Wang S, Fernandez C, A Hybrid Data Driven Framework Considering Feature Extraction for Battery State of Health Estimation and Remaining Useful Life Prediction, *Green Energy and Intelligent Transportation*, <https://doi.org/10.1016/j.geits.2024.100160>.

This is a PDF file of an article that has undergone enhancements after acceptance, such as the addition of a cover page and metadata, and formatting for readability, but it is not yet the definitive version of record. This version will undergo additional copyediting, typesetting and review before it is published in its final form, but we are providing this version to give early visibility of the article. Please note that, during the production process, errors may be discovered which could affect the content, and all legal disclaimers that apply to the journal pertain.

© 2024 Published by Elsevier Ltd on behalf of Beijing Institute of Technology Press Co., Ltd.



A Hybrid Data Driven Framework Considering Feature Extraction for Battery State of Health Estimation and Remaining Useful Life Prediction

ABSTRACT: Battery life prediction is of great significance to the safe operation, and reduces the maintenance costs. This paper proposes a hybrid framework considering feature extraction to achieve more accurate and stable life prediction performance of the battery. By feature extraction, eight features are obtained to fed into the life prediction model. The hybrid framework combines variational mode decomposition, the multi-kernel support vector regression model and the improved sparrow search algorithm to solve the problem of data backward, uneven distribution of high-dimensional feature space and the local escape ability, respectively. Better parameters of the estimation model are obtained by introducing the elite chaotic opposition-learning strategy and adaptive weights to optimize the sparrow search algorithm. The algorithm can improve the local escape ability and convergence performance and find the global optimum. The comparison is conducted by dataset from National Aeronautics and Space Administration which shows that the proposed framework has a more accurate and stable prediction performance. Compared with other algorithms, the SOH estimation accuracy of the proposed algorithm is improved by 0.16%-1.67%. With the advance of the start point, the RUL prediction accuracy of the proposed algorithm does not change much.

Keywords: State of heath; Improved sparrow search algorithm; Remaining useful life; Variational mode decomposition; Multi-kernel support vector regression; Feature extraction

Highlights:

1. A hybrid framework considering feature extraction is proposed to achieve more accurate and stable prediction performance.
2. This hybrid framework solves the problems of backward data, uneven distribution of high-dimensional feature space, and local escape ability.
3. Introducing elite chaotic opposition learning strategy and adaptive weights to improve the local escape ability and convergence performance of sparrow search algorithm, and finding the global optimal solution.
4. By feature extraction, eight features are obtained to fed into the life prediction model.

1. Introduction

Lithium-ion batteries have the characteristics of high energy density and long cycle life, and are now widely used in electric vehicles, mobile phones, laptops and other electronic products^[1]. As the number of charges and discharges increases, the battery performance continues to decline, manifested by a decrease in capacity and an increase in internal resistance. It is characterized by state of health (SOH) and remaining useful life (RUL)^[2-4]. In this paper, the ratio of the current available capacity to the rated capacity of the battery is used to express the battery . The expression of SOH is as follows:

$$SOH_n = Q_n / Q_N \quad (1)$$

Where, Q_n represents the actual battery capacity during the n th charging and discharging cycle; Q_N represents the rated battery capacity. RUL prediction reflects the long-term battery life prediction, which can ensure its safety and stability during the whole life cycle and provide information for battery replacement. Battery capacity is easier to measure and more meaningful than impedance or internal resistance, which is adopted as the SOH definition in this study.

43 1.1. Literature review

44 Battery SOH estimation and RUL prediction methods are divided into model-based and data-
45 driven methods [5]. Model-based methods can achieve life prediction though different models
46 combined with the filtering algorithm such as unscented Kalman filter (UKF) algorithm, particle
47 filter (PF) algorithm and some improved PF algorithms [6-9]. Dual exponential model is the most
48 commonly used model. As the number of iterations increases, the diversity of particles will
49 disappear and lead to the phenomenon of particle degradation. Improvement of importance density
50 function and resampling method can solve this problem and improve the prediction accuracy [10-13].
51 In literature [14], a framework combined improved ant lion optimization algorithm and support
52 vector regression is proposed to solve the degeneracy phenomenon of the standard PF method. It
53 achieves prediction results with high accuracy and robustness. The PF and improved PF algorithms
54 have good prediction accuracy and can describe the uncertainty of the battery with the probability
55 distribution function (PDF). However, model-based methods depend on the battery capacity model,
56 while there is no accurate and universal model, the results will be affected. Data-driven methods
57 such as artificial neural networks (ANN) algorithm [15-17], long short-term memory neural network
58 (LSTM) [18] and support vector machines (SVM) algorithm [19-22] have received widespread attention
59 at present. A new framework combined partial incremental capacity and ANN is proposed in [23]
60 for battery life prediction to get a good performance with better generalization ability and higher
61 prediction accuracy. However, lots of data and time are needed to train the ANN models. SVM as a
62 kind of machine learning algorithms, can be used for recognition and classification. The efficiency
63 of regression convergence is higher than other machine learning algorithms and suitable for small
64 sample prediction. Zhao et al. [24] develops a method combining the feature vector and SVR
65 algorithms for battery SOH estimation. Although the prediction accuracy is higher than that of
66 standard SVR algorithm, it still fails to solve the problem of super parameter optimization. Hybrid
67 algorithms of SVR model and parameter optimization algorithms can make better use of their
68 respective advantages and overcome the limitations of SVR model [25-27]. In reference [28], the
69 particle swarm optimization (PSO) is applied to obtain optimized parameters of SVR model for a
70 better battery RUL prediction. However, PSO algorithm cannot handle discrete optimization
71 problems well and easily lead to local optimization. An artificial bee colony (ABC) algorithm is
72 designed in reference [29] to identify the parameters of SVR model to solve the problem of local
73 optimization and improves the prediction accuracy to a certain extent. In addition, in actual
74 operation situation, the battery is affected by a lot of noise produced by its own physical
75 characteristics and the environment, which is not considered in many articles. In order to reduce this
76 random noise interference, research on signal processing methods are conducted. In reference [30],
77 the empirical model decomposition (EMD) algorithm is proposed to decompose the non-stationary
78 signals for noise reduction. However, the EMD method exists the problems of end effect and modal
79 component. The variational mode decomposition (VMD) can overcome problems above to reduce
80 the non-stationarity of time series.

81 1.2 Contributions of this paper

82 In this study, a hybrid framework considering feature extraction is proposed for a better SOH
83 estimation and RUL prediction performance. The hybrid framework combining VMD, improved
84 sparrow search algorithm (ISSA) and multi-kernel support vector regression (MKSVR) model. The
85 contributions are summarized. First, eight features are obtained to fed into the life prediction model
86 by feature extraction. Secondly, VMD method is applied to decompose the original data to make the
87 capacity data more stable. Then, elite chaotic opposition-learning strategy and adaptive weights are
88 adopted to optimize the traditional sparrow search algorithm (SSA) to obtain more accurate
89 parameters of the prediction model. Finally, MKSVR is used to solve the low prediction accuracy
90 problem caused by large sample data and uneven distribution of high-dimensional feature space.

91 1.3. Organization of the paper

92 The remainder of this article is listed as follows. Section II introduces the VMD decomposition,
93 the MKSVR model, the ISSA algorithm for parameters optimization and the hybrid VMD-ISSA-

94 MKSVR framework. Section III discusses experimental results and analysis of the proposed method.
95 Conclusions are summarized in Section IV.

96 2. Basic theories

97 2.1 Variational mode decomposition

98 VMD is used for completely non-recursive modal variation to deal with signals [31,32]. The
99 optimal solution of the variational problem is obtained finally by effective decomposition
100 component of the given signal. By iteration, the VMD algorithm can decompose the signals into
101 some intrinsic mode functions (IMFs) and a relevant residual value containing multiple different
102 frequency scales.

103 The constrained variational expression of VMD is as follows:

$$104 \min_{\{Q_m\}, \{\omega_m\}} \left\{ \sum_{m=1}^M \left\| \partial_N \left[(\delta(N) + j / \pi N) * Q_m(N) \right] \exp(-j\omega_m N) \right\|_2^2 \right\}, \quad (2)$$

$$s.t. \sum_{m=1}^M Q_m = f$$

105 where M is the number of modes to be decomposed, $\{Q_m\} = \{Q_1, Q_2, \dots, Q_M\}$ is the set of M modal
106 components after decomposition, $\{\omega_m\} = \{\omega_1, \omega_2, \dots, \omega_M\}$ is the set of center frequencies
107 corresponding to modal component, Q_m is the m -th modal component, ω_m is the center frequency of
108 m -th modal component, N is the number of sequences, $\delta(t)$ represents the dirac function.

109 The unconstrained variational expression is shown below by introducing the Lagrangian
110 multiplication operator λ :

$$111 L(\{Q_m\}, \{\omega_m\}) = \alpha \sum_{m=1}^M \left\| \partial_N \left[(\delta(N) + j / \pi N) * Q_m(N) \right] \exp(-j\omega_m N) \right\|_2^2$$

$$+ \left\| f(N) - \sum_m Q_m(N) \right\|_2^2 + \left\langle \lambda(N), f(N) - \sum_m Q_m(N) \right\rangle \quad (3)$$

112 where α is a secondary penalty factor.

113 By alternating direction multiplier iterative algorithm to obtain M modal components, the
114 unconstrained variational problem can be solved. The update expressions of Q_m , ω_m and λ are shown
115 as follows:

$$\hat{Q}_m^{k+1}(\omega) = \frac{\hat{f}(\omega) - \sum_{i=1}^m \hat{Q}_i^{k+1}(\omega) - \sum_{i=m+1}^M Q_i^k(\omega) + \hat{\lambda}(\omega) / 2}{1 + 2\alpha(\omega - \omega_m^k)^2}$$

$$116 \omega_m^{k+1} = \frac{\int_0^\infty \omega \left| \hat{Q}_m^{k+1}(\omega) \right|^2 d\omega}{\int_0^\infty \left| \hat{Q}_m^{k+1}(\omega) \right|^2 d\omega} \quad (4)$$

$$\hat{\lambda}^{k+1}(\omega) = \hat{\lambda}^k(\omega) + \gamma \left(\hat{f}(\omega) - \sum_{m=1}^M \hat{Q}_m^{k+1}(\omega) \right)$$

117 where γ is the update coefficient for Lagrangian multiplier which represents noise tolerance. $\hat{Q}_m(\omega)$,
118 $\hat{Q}_i(\omega)$, $\hat{f}(\omega)$ and $\hat{\lambda}(\omega)$ are Fourier transforms of \hat{Q}_m , \hat{Q}_i , \hat{f} and $\hat{\lambda}$.

119 The process of VMD algorithm is summarized as follows:

120 Step 1: Initialize three parameters \hat{Q}_m^1 , ω_m^1 , $\hat{\lambda}^1$ and set the iteration count to $k=1$.

121 Step 2: Update \hat{Q}_m , ω_m and $\hat{\lambda}$ by equation (4).

122 Step 3: For a specified acceptable tolerance $\xi > 0$, the convergence criterion is
 123 $\sum_{m=1}^M \|\hat{Q}_m^{k+1}(\omega) - \hat{Q}_m^k(\omega)\|_2^2 / \|\hat{Q}_m^k(\omega)\|_2^2 < \xi$. If the convergence is realized, finish the iteration and
 124 output the final value, else return to step 2.

125 2.2 Multi-Kernel Support vector regression

126 In 1995, SVM algorithm based on statistical learning theory was proposed by Vapnik. It is
 127 mainly used to obtain the global optimal solution for pattern recognition and classification. To
 128 reduce the parameter dimension, the optimization process is simplified by introducing the kernel
 129 function. When used as a regression tool, SVM implements a variant of the algorithm called SVR.

130 A set of data $T = \{(x_1, y_1), (x_2, y_2), \dots, (x_n, y_n)\}$ is given, where $x_i \in \mathbb{R}^n$, $y_i \in \mathbb{R}^n$, $\{x_i, i=1, 2, \dots, n\}$ is the
 131 input feature, $\{y_i, i=1, 2, \dots, n\}$ is the output. The target of SVR method is to find a functional
 132 relationship similar to the hyperplane equation $f(x)$, making it as close to the training data as possible.
 133 In the feature space, the regression model corresponding to the hyperplane can be described as the
 134 equation (5):

$$135 \quad f(x) = w_s^T \varphi(x) + b_s \quad (5)$$

136 where $\varphi(x)$ is a nonlinear mapping function, w_s is the normal vector, b_s is the displacement term.

137 The optimization problem of SVR model can be expressed as:

$$138 \quad \begin{aligned} & \min \frac{1}{2} \|w_s\|^2 + C \sum_{i=1}^n (\xi_i + \hat{\xi}_i) \\ & s.t. (w_s^T \varphi(x_i) + b_s - y_i) \leq \varepsilon + \xi_i, \\ & y_i - w_s^T \varphi(x_i) - b_s \leq \varepsilon + \hat{\xi}_i, \xi_i \geq 0, \hat{\xi}_i \geq 0, i = 1, 2, \dots, n \end{aligned} \quad (6)$$

139 where ε is the regression error, similar to relaxation factor, which introduces outliers into the support
 140 vector. C is the penalty constant.

141 Four Lagrangian multipliers α_i , α_i^* , u_i and u_i^* are introduced to obtain Lagrangian function:

$$142 \quad \begin{aligned} L(w_s, b_s, \alpha_i, \alpha_i^*) &= \frac{1}{2} \|w_s\|^2 + C \sum_{i=1}^n (\xi_i + \hat{\xi}_i) - \sum_{i=1}^n \mu_i \xi_i - \sum_{i=1}^n \mu_i^* \hat{\xi}_i \\ &+ \sum_{i=1}^n \alpha_i (w_s^T \cdot \varphi(x_i) + b_s - \xi_i - \varepsilon - y_i) + \sum_{i=1}^n \alpha_i^* (y_i - w_s^T \cdot \varphi(x_i) - b_s - \hat{\xi}_i - \varepsilon) \end{aligned} \quad (7)$$

143 where $\alpha_i \geq 0$, $\alpha_i^* \geq 0$, $u_i \geq 0$ and $u_i^* \geq 0$.

144 The SVR regression model can be finally transformed as the function below:

$$145 \quad f(x) = w_s^T \cdot x + b_s = \sum_{i=1}^n \sum_{j=1}^n (\alpha_i^* - \alpha_i) K(x_i, x_j) + b_s \quad (8)$$

146 where $K(x_i, x_j)$ is the Gaussian radial basis kernel function, the expression of which is
 147 $K(x_i, x_j) = \exp(-\frac{\|x_i - x_j\|^2}{2\sigma^2})$. The kernel function can improve the Feature dimension of the model to
 148 improve the nonlinear fitting ability of SVR. The larger the σ is, the smaller the nonlinear efficiency
 149 is, and the less sensitive to noise is.

150 When the amount of sample data is large, the distribution of high-dimensional feature space is
 151 uneven and there is heterogeneous information, a single selection of local kernel function or global
 152 kernel function will lead to low prediction accuracy. This problem can be solved by constructing
 153 multi-kernel functions by linear weighting.

154 By combining the linear kernel function with the Gaussian kernel function, the multi-kernel
 155 function can be expressed as:

$$156 \quad K(x_i, x_j) = \lambda k_1(x_i, x_j) + (1 - \lambda) k_2(x_i, x_j) \quad (9)$$

157 where $k_1(x_i, x')$ is a linear kernel function, $k_2(x_i, x')$ is Gaussian kernel function. λ is the
 158 weight coefficient of linear kernel function, and the corresponding $(1-\lambda)$ is the weight coefficient of
 159 Gaussian kernel function.

160 2.3 Improved sparrow search algorithm

161 The SSA is a new type of swarm intelligence optimization algorithm, and its basic structure
 162 is similar to ABC algorithm except the search operator [33]. In this paper, SSA algorithm is used to
 163 optimize penalty constant C and kernel function parameter σ to realize the accurate prediction of
 164 the MKSVM model.

165 For SSA algorithm, each sparrow has only one position, which can be represented by a matrix
 166 X , and the expression is:

$$167 \quad X = \begin{bmatrix} x_{1,1} & x_{1,2} & \cdots & x_{1,d} \\ x_{2,1} & x_{2,2} & \cdots & x_{2,d} \\ \cdots & \cdots & \cdots & \cdots \\ x_{n,1} & x_{n,2} & \cdots & x_{n,d} \end{bmatrix} \quad (10)$$

168 where d is the dimension of the variable. x_{ij} indicates the position of the i -th sparrow in the j -th
 169 dimension.

170 The fitness value is calculated by:

$$171 \quad F_X = \begin{bmatrix} f([x_{1,1} & x_{1,2} & \cdots & x_{1,d}]) \\ f([x_{2,1} & x_{2,2} & \cdots & x_{1,d}]) \\ \cdots \\ f([x_{n,1} & x_{n,2} & \cdots & x_{n,d}]) \end{bmatrix} \quad (11)$$

172 Each sparrow has three possible behaviors: explorer, follower, and vigilant investigation. Each
 173 generation selects the best P sparrows in the population as the explorers, and the remaining $n-P$
 174 sparrows as the followers.

175 The position update equation is:

$$176 \quad X_{i,j}^{t+1} = \begin{cases} X_{i,j}^t \cdot \exp\left(\frac{-i}{\alpha \cdot M}\right), R_2 < ST \\ X_{i,j}^t + Q_s \cdot L_s, R_2 \geq ST \end{cases} \quad (12)$$

177 where t is the number of current iteration, M is the maximum iterations number. $X_{i,j}^t$ indicates the
 178 position of the i -th sparrow in the j -th dimension of the current iteration. α is a random number
 179 between 0 and 1. R_2 is the alarm value and ST is the safety threshold. Q is a random number. L is a
 180 $1 \times d$ matrix with each element of 1.

181 The location updated equation is:

$$182 \quad X_{i,j}^{t+1} = \begin{cases} \exp\left(\frac{X_{wp}^t - X_{i,j}^t}{i^2}\right) \cdot Q_s, i > n/2 \\ |X_{i,j}^t - X_{bp}^{t+1}| \cdot G_s^+ \cdot L_s + X_{bp}^{t+1}, i \leq n/2 \end{cases} \quad (13)$$

183 where X_{bp} is the best position occupied by the current explorer, X_{wp} is the worst position. G represents
 184 a $1 \times d$ matrix with elements assigned 1 or -1 and $G^+ = G^T(GG^T)^{-1}$.

185 While the sparrows are foraging for food, part of them will be responsible for vigilance. When
 186 alerted to danger, they will conduct anti-predation behavior: give up food and move to a new
 187 location. The location update formula is:

$$X_{i,j}^{t+1} = \begin{cases} X_{bp}^t + \mu_s \cdot |X_{i,j}^t - X_{bp}^t|, f_{si} > f_{sg} \\ X_{i,j}^t + K_s \cdot \left(\frac{|X_{i,j}^t - X_{wp}^t|}{(f_{si} - f_{sw}) + \zeta} \right), f_{si} = f_{sg} \end{cases} \quad (14)$$

where X_{bp} is the current global optimal position, μ_s is the step-size control parameter, K is the random with values between -1 and 1, which represents the moving direction of the sparrows. f_{si} is the fitness value of the current sparrow. f_{sg} represents current global best fitness value while f_{sw} represents the worst one. ζ is a minimum constant.

2.3.1 Improvement of population initialization

Elite chaotic opposition-learning method is adopted to generate an initial population to enhance its quality and diversity. By selecting elite individuals on a larger scale, the algorithm can improve the local escape ability and convergence performance of traditional SSA algorithm, then lead to a more accurate solution.

In this paper, the chaotic skew tent map is chosen to generate the initial population to enhance the stability of the initial individuals due to its characteristic of randomness and ergodicity.

The chaotic skew tent map equation is described as follows:

$$x_{k+1} = \begin{cases} x_k / \alpha, 0 < x_k < \alpha \\ (1 - x_k) / (1 - \alpha), \alpha < x_k \leq 1 \end{cases} \quad (15)$$

In (15), α is a random number between 0 and 1. $\beta = -\alpha \log \alpha - (1 - \alpha) \log (1 - \alpha)$, if $\beta > 0$, then the system is in chaos state.

The reverse-learning algorithm based on optical lens imaging principle can solve the problem of local optimum by increasing the probability of a better solution.

Reverse population generation equation is described in (16):

$$x_n^* = \frac{a_n + b_n}{2} + \frac{a_n + b_n}{2k} - \frac{x_n}{k} \quad (16)$$

where a_n represents the minimum value in the n dimension of the current population, while b_n represents the maximum one. k is the scaling coefficient of the lens.

The initialize process of the sparrow population with the strategy above is shown as as follows:

Initialize the sparrow population randomly, then substitute population X into equation (15) to generate chaotic population Y. Generate the lens imaging opposition-learning population Z by substituting population X into equation (16). Sort the population X、Y and Z according to the individual fitness value and select the better N individuals to form the initial sparrow population.

2.3.2 Improvement of follower location update

Since the update weight is large and not changed much during iteration, it may miss the global optimum. To solve the problem, adaptive weights are introduced to improve the performance of SSA algorithm.

The changed update equation is described as follows:

$$X_{i,j}^{t+1} = \begin{cases} w_s \cdot \left(X_{i,j}^t \cdot \exp\left(\frac{-i}{\alpha_s \cdot Iter_{\max}}\right) \right) & \text{if } AR < ST \\ w_s \cdot (X_{i,j}^t + Q_s L_s) & \text{if } AR \geq ST \end{cases} \quad (17)$$

$$w_s = 1 - \lg\left(\frac{(e-1) \cdot n}{Iter_{\max}} + 1\right)$$

221 2.4 A hybrid framework of VMD-ISSA-MKSVR

222 A hybrid framework combining VMD, ISSA and MKSVR model is proposed to achieve a more
 223 accurate and stable battery life prediction performance. The detailed prediction process is outlined
 224 in Figure 1.

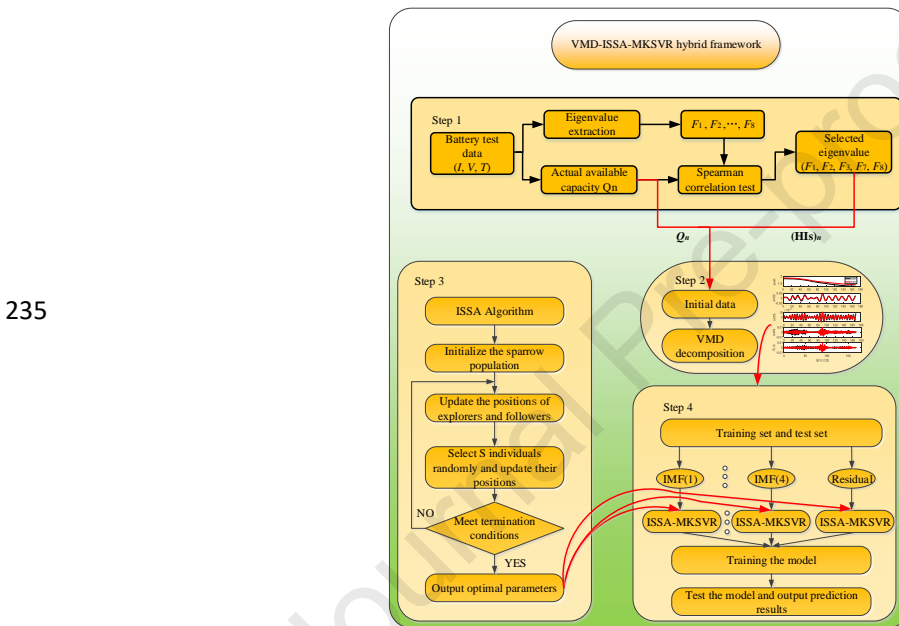
225 The complete steps of the framework are summarized as follows.

226 Step 1: Some relevant features are extracted from current, voltage, and temperature curves.
 227 Then, features with high correlation are used as the input of VMD-ISSA-MKSVR model.

228 Step 2: Decompose the battery capacity by the VMD into 5 IMF components. Each component
 229 is processed to the VMD-ISSA-MKSVR model separately, and finally put it together.

230 Step 3: After VMD decomposition, ISSA algorithm is used to identify the parameters of
 231 MKSVR model.

232 Step 4: Train the VMD-ISSA-MKSVR model, and then substitute the test data into the training
 233 model for SOH estimation and RUL prediction results.
 234



236 Fig. 1 Detailed flow chart of the hybrid framework

237 3. Experimental results and analysis

238 Four lithium-ion batteries (B0005, B0006, B0007 and B00018) from NASA are selected for
 239 SOH estimation and RUL prediction verification. The tests are carried out at room temperature,
 240 taking B0005 battery as an example: Charge the battery with a current of 1.5A in a constant current
 241 (CC) mode until it reaches the charging cut-off voltage of 4.2V. Then charge the battery by constant
 242 voltage (CV) mode with the voltage of 4.2V, stop charging when the current drops to 0.02A. During
 243 discharging, the battery is discharged in a CC mode, the discharging current is 2A, stop discharging
 244 when the discharge cut-off voltage of 2.7V is reached.

245 3.1 Evaluation criteria

246 For battery SOH estimation, this paper uses three popular criteria to verify the stability and
 247 accuracy of the model. Mean absolute error (MAE), root mean square error (RMSE), and mean
 248 absolute percentage error (MAPE) are adopted as evaluation criteria.

$$MAE = \frac{1}{M} \sum_{n=1}^M |y_n^* - y_n|$$

249

$$RMSE = \sqrt{\frac{1}{M} \sum_{n=1}^M (y_n^* - y_n)^2} \quad (18)$$

$$MAPE = \frac{1}{M} \sum_{n=1}^M \left| \frac{y_n^* - y_n}{y_n} \right| \times 100\%$$

250

Relative error (RE) is define as equation(19) for battery RUL prediction:

251

$$RE = \left| RUL_p - RUL_t \right| \quad (19)$$

252

where RUL_p is the predicted value of RUL, RUL_t is the actual value of RUL.

253

3.2 Feature extraction

254

The battery capacity cannot be obtained directly in practical. Some key features can be extracted from the current, voltage and temperature in the process of charging-discharging. It is easy to extract stable feature information from vehicle sensors to establish the relationship with battery SOH, and then use machine learning technology to realize battery life prediction.

258

259

260

261

262

263

264

265

266

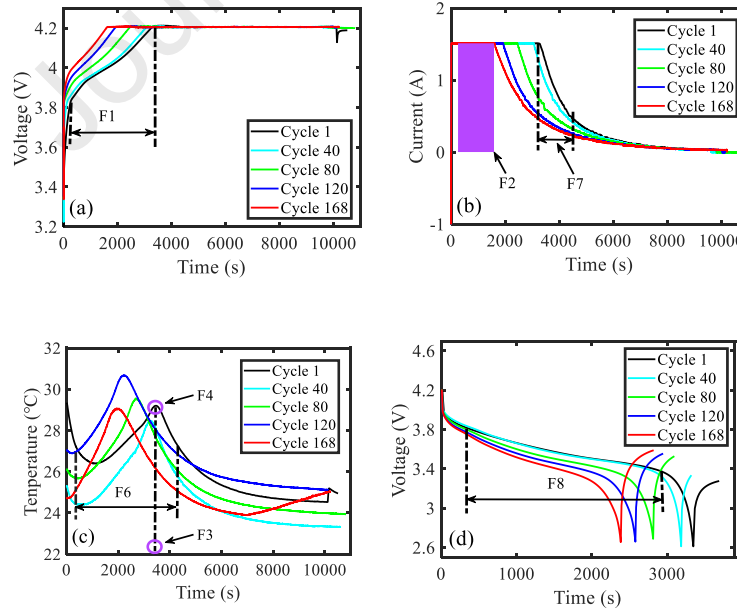
267

268

269

In the process of battery operation, the voltage curve can provide a lot of information related to the available capacity. Time interval of equal charge voltage rise (TIE-CVR), charge capacity rise of equal charge voltage rise (CCR-CVR) and time interval of equal charge current drop (TIE-CCD) can be used as features to estimate battery SOH. TIE-CVR indicates the time for the voltage to rise from 3.8V to 4.2V during CC mode charging, which is marked as F1. The corresponding capacity of CCR-CVR is marked as F2. The highest temperature and the corresponding time in each charging-discharging cycle are marked as F3 and F4, respectively. During the period when the voltage is higher than 3.8V and the current drops to 0.4A, the average temperature is recorded as F5. The area under the temperature curve is recorded as F6. TIE-CCD is the time when the current in the CV phase decreases from 1.5A to 0.4A, which is marked as F7. During the period when the discharge voltage decreases from 3.8V to 3.4V, the capacity of the discharged battery is recorded as F8. Figure 3 shows the eigenvalue of F1~F8.

270



271

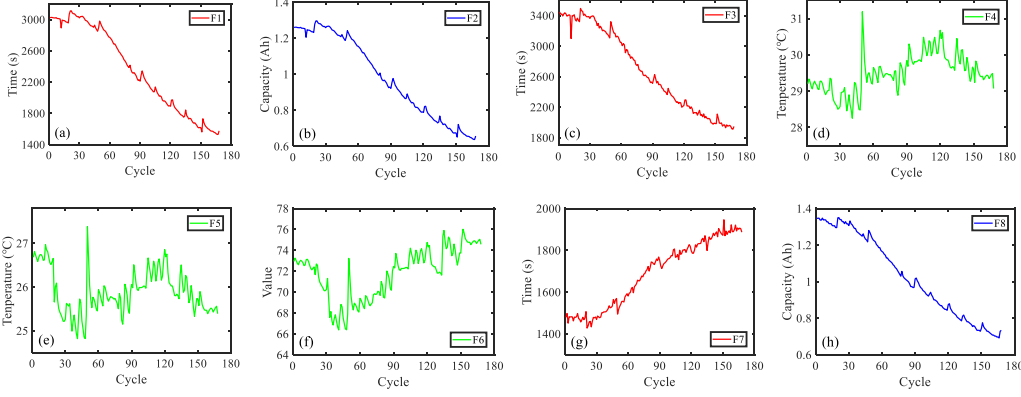
272

Fig. 2 Schematic diagram of extraction of eight eigenvalues at current, voltage and temperature (a) F1

273

(b) F2 and F7 (c) F3, F4 and F6 (d) F8

274



275

276

Fig. 3 The variation curve of eight characteristics (a)-(h) are F1-F8, respectively

277

The spearman rank correlation coefficients R_s is used to analyze the correlation between eigenvalues and battery available capacity.

278

279

The formula is shown in (20):

280

$$R_s = \frac{\sum_{n=1}^M (X_n - \bar{X})(Y_n - \bar{Y})}{\sqrt{\sum_{n=1}^M (X_n - \bar{X})^2} \sqrt{\sum_{n=1}^M (Y_n - \bar{Y})^2}} \quad (20)$$

$$\bar{X} = \frac{1}{M} \sum_{n=1}^M X_n$$

281

where X_n is the available capacity for each discharge, Y_n is the input eigenvalues in each charge-discharge cycle, \bar{X} and \bar{Y} are the mean values of sample, n is the current charge-discharge cycle, M is the total number of charge and discharge cycles.

282

283

284

Table 1 depicts the correlation coefficient between each feature and available capacity.

285

286

287

288

289

Among the four batteries, the absolute values of the correlation coefficients between F1, F2, F3, F7, and F8 and the available capacity are all between 0.9 and 1, indicating a high correlation between them. The correlation values of eigenvalues F4, F5 and F6 with available capacity are all low, indicating that their correlation is also relatively low. These three features are eliminated, and not used as input to the estimation model.

290

Table 1. Correlation coefficient between each feature and available capacity.

Battery number	Feature number							
	F1	F2	F3	F4	F5	F6	F7	F8
B0005	0.9913	0.9913	0.9911	-0.5880	0.0717	-0.6251	-0.9819	0.9987
B0006	0.9936	0.9936	0.9915	-0.1562	0.1647	0.1040	-0.9522	0.9992
B0007	0.9888	0.9888	0.9897	-0.4535	0.0379	-0.0712	-0.9444	0.9972
B0018	0.9782	0.9782	0.9823	-0.2631	0.7084	0.2127	-0.9128	0.9986

291

292

3.3 SOH estimation

293

294

295

296

Before SOH estimation, the VMD method is used to decompose the data. The VMD decomposition diagram of B0005 and B0007 is shown in figure 4. Each data is divided into five components, The frequencies of five components are different. The component frequencies of B0005 and B0007 are similar.

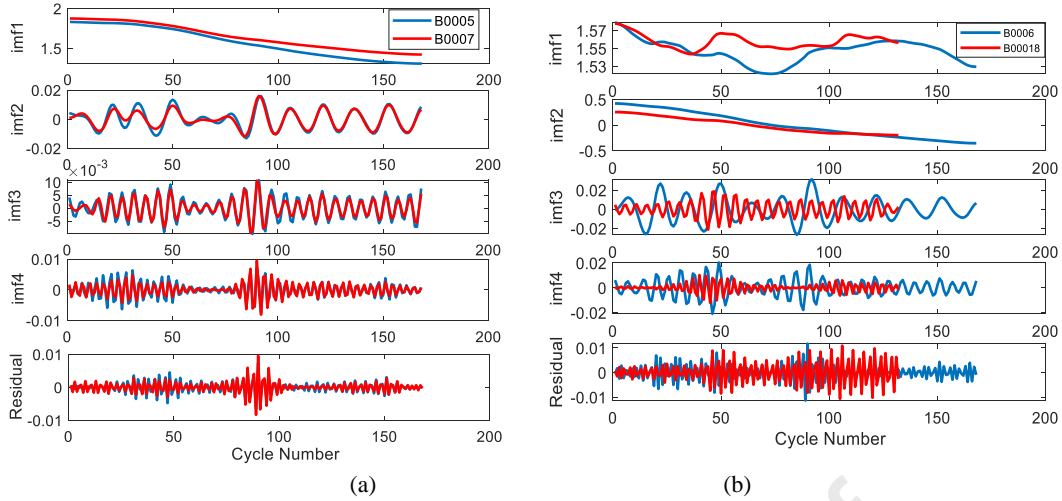


Fig. 4 Battery capacity estimation results VMD decomposition of capacity data (a) B0005 and B0007 (b) B0006 and B00018

In this paper, the capacity-based SOH definition method is adopted, which is defined as the ratio of the current capacity to the rated capacity of the battery. For the same battery, its rated capacity is constant, and the current capacity and SOH have the same trend. The problem of SOH estimation of the battery can be transformed into the problem of capacity estimation.

For SOH estimation, the characteristic factors are extracted as the input of VMD-ISSA-MKSVR model. The prediction start point of B0005, B0006 and B0007 is $T_y=81$, while that of B00018 is $T_y=61$. The data before the starting point is set as the training set, and the data after the starting point is set as the test set.

Four methods including the IPSO-SVR^[34], ISSA-SVR, VMD-ISSA-SVR and BL-ELM^[35] are in comparison with VMD-ISSA-MKSVR for battery SOH estimation. The relevant parameters are set in table 2. The kernel parameters are Obtained by three optimization methods listed as table 3.

To verify the effectiveness of the proposed method for SOH estimation, a comparison of the battery capacity estimation is conducted as shown in Figure 5. The SOH estimation results clearly show that the conformance between estimation and measurement are adequate. The capacity estimation values all follow the actual value, and the errors are quite small. Compared with the capacity obtained by the IPSO-SVR and ISSA-SVR, that obtained by the VMD-ISSA-SVR and the VMD-ISSA-MKSVR are closer to the actual capacity.

Table 2. The parameter setting

Algorithm	Parameters
IPSO-SVR	$N=100$, $Iter_{max}=100$,
ISSA-SVR	$N=100$, $Iter_{max}=100$,
VMD-ISSA-SVR	$N=100$, $Iter_{max}=100$
BL-ELM	$N=100$, $Iter_{max}=100$
VMD-ISSA-MKSVR	$N=100$, $Iter_{max}=100$

Table 3 The kernel parameters are Obtained by three optimization methods

Algorithm	B0005	B0006	B0007	B00018
IPSO-SVR	$\sigma=0.01$	$\sigma=0.01$	$\sigma=0.01$	$\sigma=0.01$
ISSA-SVR	$\sigma=0.0122$	$\sigma=0.01$	$\sigma=0.01$	$\sigma=0.5414$
VMD-ISSA-SVR	$\sigma=404.72$	$\sigma=337.7$	$\sigma=1386$	$\sigma=512.9$

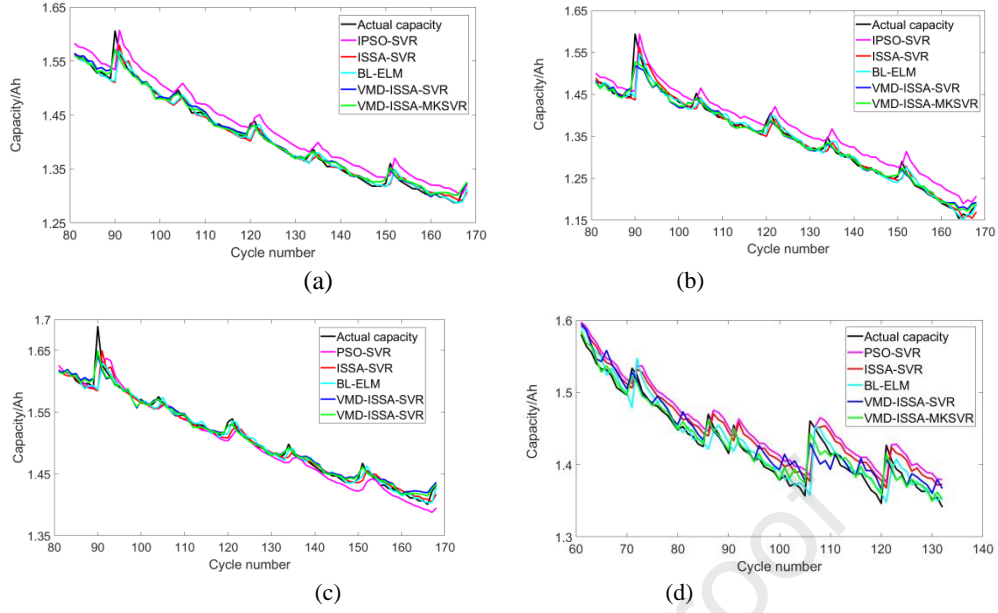


Fig. 5 Battery capacity estimation results(a)B0005 (b)B0006 (c)B0007 (d)B00018

Table 4. Battery capacity estimation error

Battery	Algorithm	MAE (%)	RMSE (%)	MAPE
B0005	IPSO-SVR[34]	2.1603	2.331	1.3453%
	BL-ELM[35]	0.650599	1.28178	0.469636%
	ISSA-SVR	0.70846	1.3541	0.50759%
	VMD-ISSA-SVR	0.64732	0.85372	0.4553%
	VMD-ISSA-MKSVR	0.48948	0.66529	0.34572%
B0006	IPSO-SVR[34]	2.818	2.6655	1.5552%
	BL-ELM[35]	0.907669	1.89784	0.692424%
	ISSA-SVR	0.93202	2.0196	0.71344%
	VMD-ISSA-SVR	0.84719	1.2776	0.6403%
	VMD-ISSA-MKSVR	0.70188	1.0757	0.53136%
B0007	IPSO-SVR[34]	0.9444	1.6086	0.55921%
	BL-ELM[35]	0.552247	1.25203	0.374816%
	ISSA-SVR	0.67	1.38	0.455%
	VMD-ISSA-SVR	0.55814	0.81174	0.37043%
	VMD-ISSA-MKSVR	0.43931	0.65092	0.29301%
B00018	IPSO-SVR[34]	2.8662	3.0179	1.814%
	BL-ELM[35]	1.27736	2.00969	0.896704%
	ISSA-SVR	2.2697	2.5105	1.5769%
	VMD-ISSA-SVR	1.6407	1.3489	0.93712%
	VMD-ISSA-MKSVR	1.2713	1.1008	0.88236%

MKSVR

327 The capacity estimation error is shown in Table 4 and Figure 6. Take B0005 battery as an
 328 example, the MAE of the five methods are 2.1603%, 0.708%, 0.651%, 0.647% and 0.489%,
 329 respectively, while the RMSE of that are 2.331%, 1.354%, 1.282%, 0.854% and 0.665%,
 330 respectively; and the MAPE of that are 1.345%, 0.508%, 0.470%, 0.455% and 0.346%, respectively.
 331 The capacity estimation error of the IPSO-SVR is largest, that of the proposed VMD-ISSA-MKSVR
 332 method is smallest, the error reductions of MAE, RMSE, and MAPE are obvious. Compared with
 333 the results predicted by the IPSO-SVR algorithm, the proposed method improves the estimation
 334 SOH accuracy by nearly 0.51% ~ 2.11%. These results suggest that the proposed VMD-ISSA-
 335 MKSVR method has a relatively high estimation accuracy.

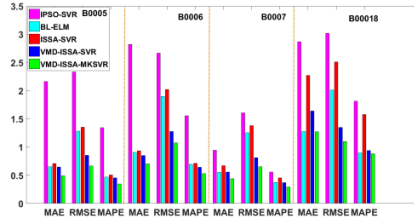


Fig. 6 Battery capacity estimation error

3.4 RUL prediction

337
 338 The battery RUL prediction results are discussed in this section. Take the cycle number as input
 339 of the prediction methods, the EOL threshold for the B0005, B0006 and B00018 batteries are set to
 340 70% of the standard rated capacity, which is 1.4Ah. The EOL threshold for the B0007 battery is set
 341 to 75% of the standard rated capacity, which is 1.5Ah. The prediction start points of the four batteries
 342 are Ty=41.
 343

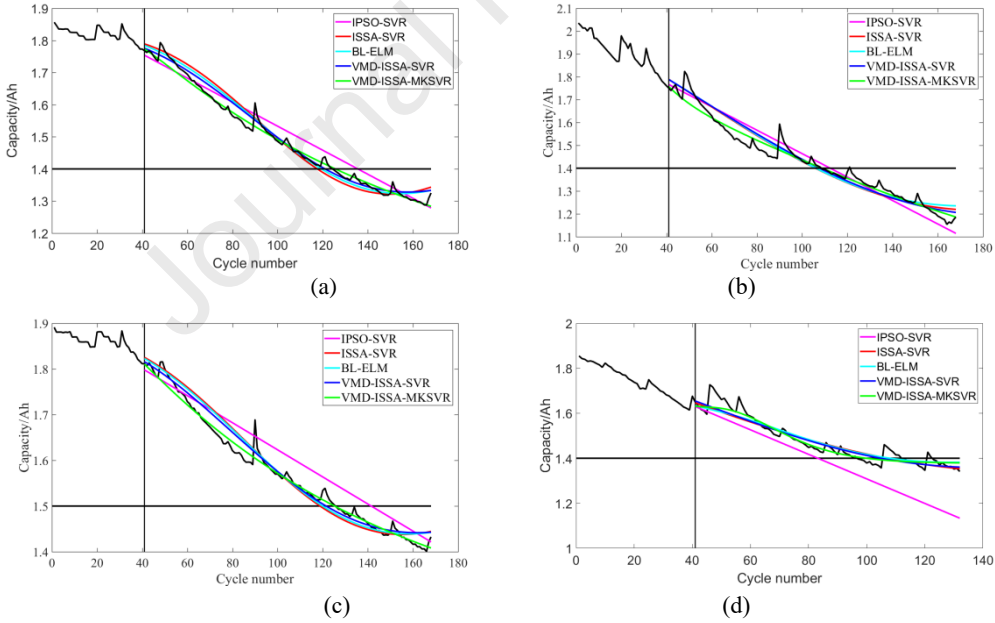


Fig. 7 Battery RUL prediction results (a)B0005 (b)B0006 (c)B0007 (d)B00018

Table 5. Battery RUL prediction error

Battery	Algorithm	Start point	RUL_p	RUL_r	RE
B0005	IPSO-SVR[34]	41	95	83	12
	BL-ELM[35]	41	78	83	5
	ISSA-SVR	41	77	83	6
	VMD-ISSA-SVR	41	80	83	3

	VMD-ISSA-MKSVR	41	84	83	1
B0006	IPSO-SVR[34]	41	72	68	4
	BL-ELM[35]	41	65	68	3
	ISSA-SVR	41	65	68	3
	VMD-ISSA-SVR	41	67	68	1
	VMD-ISSA-MKSVR	41	68	68	0
B0007	IPSO-SVR[34]	41	92	85	7
	BL-ELM[35]	41	79	85	6
	ISSA-SVR	41	78	85	7
	VMD-ISSA-SVR	41	80	85	5
	VMD-ISSA-MKSVR	41	85	85	0
B0001 8	IPSO-SVR[34]	41	67	56	11
	BL-ELM[35]	41	67	56	11
	ISSA-SVR	41	66	56	10
	VMD-ISSA-SVR	41	64	56	8
	VMD-ISSA-MKSVR	41	59	56	3

Figure 7 and Table 5 show the battery RUL prediction results. The RE of the proposed hybrid method is smaller than those of the other methods, indicating that the hybrid algorithm has a higher prediction accuracy. The RE value predicted by the IPSO-SVR for four batteries are 12, 4, 7 and 11, respectively; by the BL-ELM method those are 5, 3, 6 and 11, respectively; by the ISSA-SVR method those are 6, 3, 7 and 10, respectively; by the VMD-ISSA-SVR method those are 3, 1, 5 and 8, respectively; by the VMD-ISSA-MKSVR method those are 1, 0, 0 and 3. Especially for B00018, the RUL prediction accuracy has been greatly improved.

Table 6 RUL prediction results of four batteries with different start points

Battery	Algorithm	RE ₅₁	RE ₄₁	RE ₃₁
B0005	IPSO-SVR[34]	10	12	∞
	BL-ELM[35]	8	5	20
	ISSA-SVR	10	6	∞
	VMD-ISSA-SVR	2	3	16
	VMD-ISSA-MKSVR	2	1	10
B0006	IPSO-SVR[34]	3	4	8
	BL-ELM[35]	6	3	23
	ISSA-SVR	4	3	9
	VMD-ISSA-SVR	2	1	10
	VMD-ISSA-MKSVR	1	0	2
B0007	IPSO-SVR[34]	8	16	∞
	BL-ELM[35]	7	6	8
	ISSA-SVR	6	7	∞
	VMD-ISSA-SVR	6	5	7
	VMD-ISSA-MKSVR	4	0	5
B00018	IPSO-SVR[34]	10	14	15
	BL-ELM[35]	13	11	9
	ISSA-SVR	12	10	10
	VMD-ISSA-SVR	9	8	6
	VMD-ISSA-MKSVR	2	3	1

The RUL prediction results of four batteries with different start points are shown in table 6. ∞ in the table represents that the prediction curve and EOL do not intersect and the RUL cannot be predicted. It can be seen that the five methods can predict the RUL of the four batteries very well after $T_y=41$ and the RE values obtained by the VMD-ISSA-MKSVR method are the smallest for every battery. The RE values predicted by the five methods generally show an roughly upward trend

363 with the advancement of the start point. When $T_y=31$, the RUL predictions of B0005 and B0007
 364 batteries by IPSO-SVR and ISSA-SVR cannot be performed because of the small amount of data.
 365 The RUL errors predicted by BL-ELM, VMD-ISSA-SVR and VMD-ISSA-MKSVR are still
 366 suitable. With the advance of the start point, the prediction accuracy of the proposed hybrid method
 367 does not change much, indicating that the RUL predicted by VMD-ISSA-MKSVR method is stable.

368 4. Conclusion

369 As a key approach of prognostics and health management, accurate life prediction of the battery
 370 is significant to reduce the probability of system failure effectively. This work focus on a hybrid
 371 method considering feature extraction that combines VMD, ISSA and MKSVR.

372 The main contributions are summarized as follows:(1) Eight Features are extracted to establish
 373 the relationship with battery SOH by measured data. (2) Decompose the original sequence by the
 374 VMD to solve the backward problem of the capacity data caused by auto-correlation to make the
 375 capacity data more stable. (3) Elite chaotic opposition learning strategy and adaptive weights are
 376 introduced to optimize the SSA algorithm to find the global optimum faster and more efficient. (4)
 377 Multi-Kernel support vector regression is used to solve the low prediction accuracy problem caused
 378 by large sample data, uneven distribution of high-dimensional feature space. Training data is used
 379 to train the hybrid model, and the test data is substituted into the training model for battery life
 380 prediction results.

381 Dataset from National Aeronautics and Space Administration are applied for experimental
 382 verification. The RUL predictions with different start points are conducted to verify the stability of
 383 the VMD-ISSA-MKSVR framework. By comparison with IPSO-SVR, ISSA-SVR, BL-ELM and
 384 VMD-ISSA-SVR, it can be verified that the errors of SOH estimation and RUL prediction obtained
 385 by the VMD-ISSA-MKSVR framework are the smallest. It has relatively high prediction accuracy
 386 and stability.

387 Acknowledgments

388 I thank W.D., Y.H. for critically reading the manuscript and helpful discussions;
 389 conceptualization, Y.C.; methodology, Y.C.; software, Y.C.; validation, Y.C. and W.D.; formal
 390 analysis, Y.C. and W.D.; data curation, Y.C.; writing—original draft preparation, Y.C.; writing—
 391 review and editing, Y.C.; supervision, Y.H.; funding acquisition, Y.H.

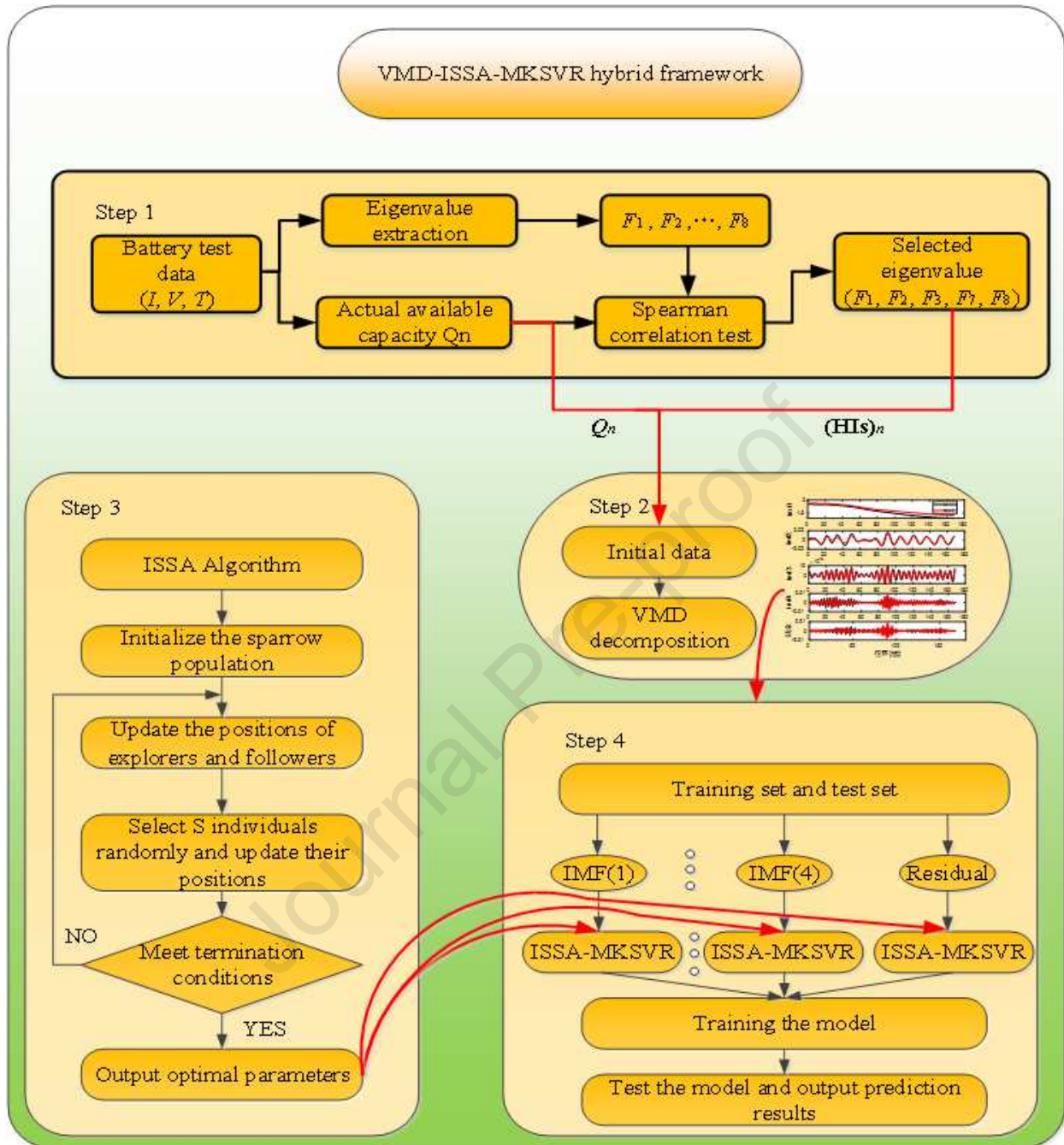
392 This work was supported by the National Natural Science Foundation of China (Grant number
 393 51577046), the State Key Program of the National Natural Science Foundation of China (Grant
 394 number 51637004), and the National Key Research and Development Plan “Important Scientific
 395 Instruments and Equipment Development” (Grant number 2016YFF0102200).

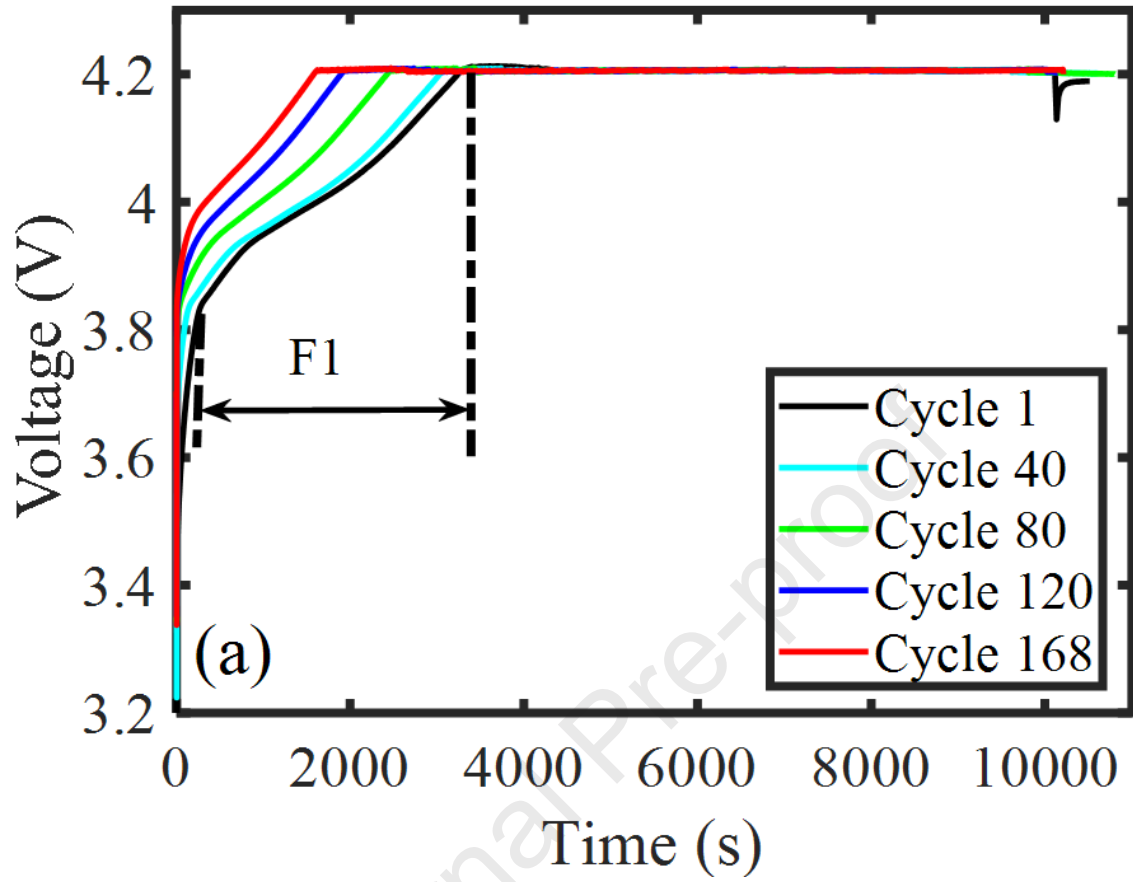
396 References

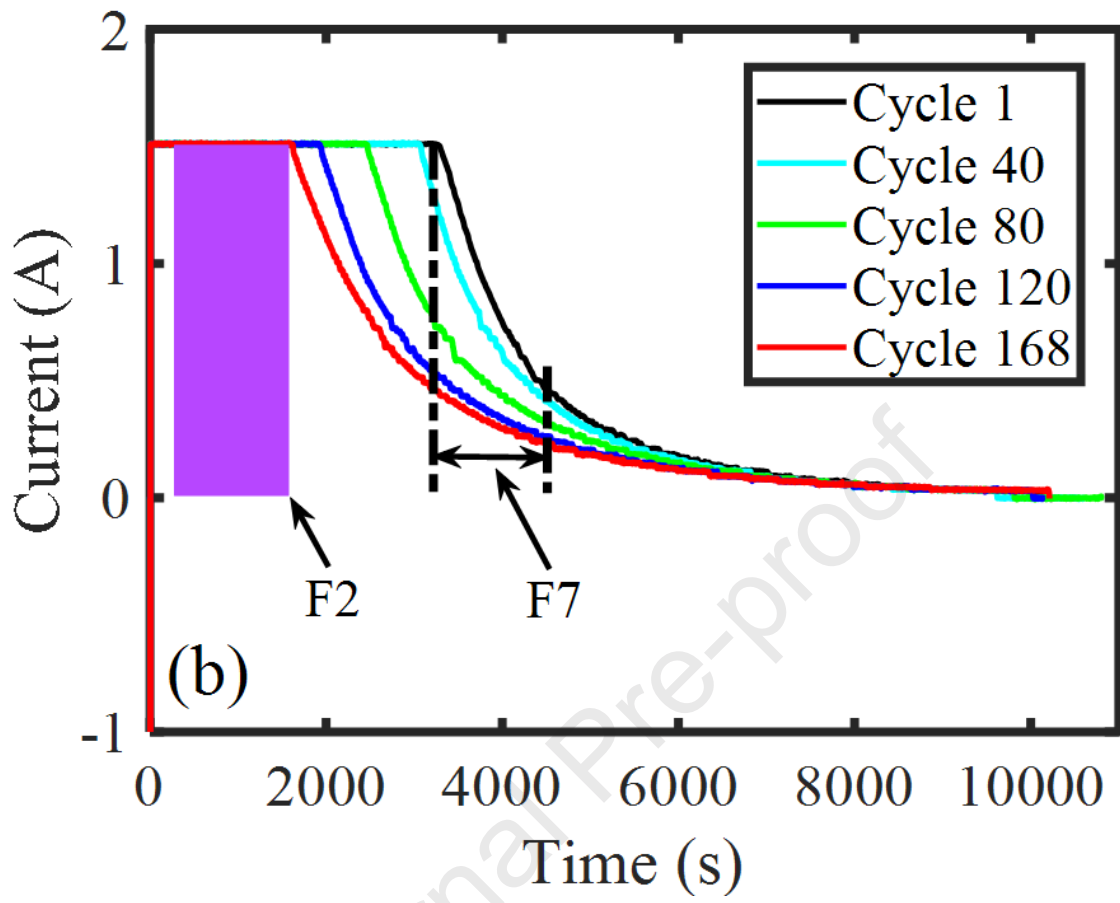
- 397 [1] Wang, S., Fernandez, C., Yu, C., Fan, Y., Stroe, D. I. A novel charged state prediction method of the lithium
 398 ion battery packs based on the composite equivalent modeling and improved splice kalman filtering
 399 algorithm[J]. Journal of Power Sources, 471, 228450.
 400 [2] Panchal S., Mathew M., Fraser R., et al. Electrochemical thermal modeling and experimental measurements of
 401 18650 cylindrical lithium-ion battery during discharge cycle for an EV[J]. Applied thermal engineering, 2018,
 402 135:123-132.
 403 [3] Li P., Zhang Z., Xiong Q., et al. State-of-health estimation and remaining useful life prediction for the lithium-
 404 ion battery based on a variant long short term memory neural network[J]. Journal of Power Sources,2020, 459.
 405 [4] Xiaoyu L., Zhang L., Wang Z. Remaining useful life prediction for lithium-ion batteries based on a hybrid
 406 model combining the long short-term memory and elman neural network[J]. The Journal of Energy Storage,
 407 2019,21: 510–518.
 408 [5] Yi A., Kang L. A., Xuan L. A., et al. Lithium-ion battery capacity estimation - A pruned convolutional neural
 409 network approach assisted with transfer learning[J]. Applied Energy, 2021, 285:116410.
 410 [6] Zheng Y., Qin C., Lai X., et al. A novel capacity estimation method for lithium-ion batteries using fusion
 411 estimation of charging curve sections and discrete Arrhenius aging model. Applied Energy, 2019, 251:113327.
 412 [7] Qin Q., Zhao S., Chen S., et al. Adaptive and robust prediction for the remaining useful life of electrolytic

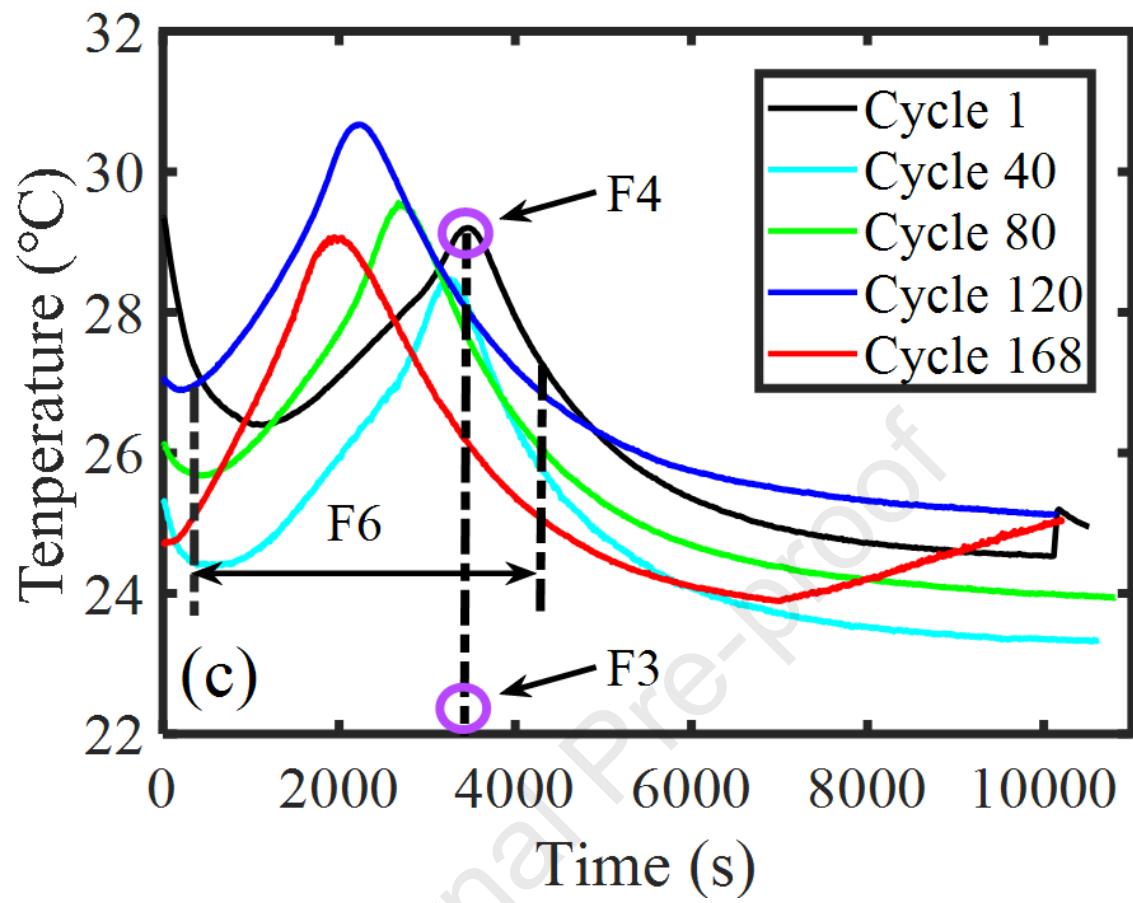
- 413 capacitors[J]. *Microelectronics & Reliability*, 2018, 87: 64-74.
- 414 [8] Dong G., Chen Z., Wei J., et al. Battery health prognosis using Brownian Motion modeling and particle
415 filtering[J]. *IEEE Transactions on Industrial Electronics*, 2018, 65(11): 8646-8655.
- 416 [9] Chang Y., Fang H. A hybrid prognostic method for system degradation based on particle filter and relevance
417 vector machine[J]. *Reliability Engineering & System Safety*, 2019, 186: 51-63.
- 418 [10] Zhu Z. Y. Improved particle filter algorithm based on importance density function selection, in *Particle Filter
419 Algorithm Its Application*, 4nd ed. BeiJing, China: Science Press, 2010: 37-38.
- 420 [11] Wei J.W., Dong G.Z., and Chen Z.H. Remaining useful life prediction and state of health diagnosis for lithium-
421 ion batteries using particle filter and support vector regression[J]. *IEEE Transactions on Industrial Electronics*,
422 2018, 65(7): 5634-5643.
- 423 [12] Mejdoubi A. E, Chaoui H., Gualous H. Lithium-ion batteries health prognosis considering aging conditions[J].
424 *IEEE Transactions on Power Electronics*, 2019, 34: 6834-6844.
- 425 [13] Chen Y., He Y. G., Li Z., et al. Remaining useful life prediction and state of health diagnosis of lithium-ion
426 battery based on second-order central difference particle filter. *IEEE ACCESS*. 2020, 8: 37305-37313.
- 427 [14] Li Q. L., Li D. Z., Zhao K., et al. State of health estimation of lithium-ion battery based on improved ant lion
428 optimization and support vector regression[J]. *Journal of Energy Storage*, 2022, 50: 104215.
- 429 [15] Pang X., Huang R., Wen J., et al. A lithium ion battery RUL prediction method considering the capacity
430 regeneration phenomenon[J]. *Energies*, 2019, 12(12).
- 431 [16] Yang H., Wang P., An Y., et al. Remaining Useful Life Prediction Based on Denoising Technique and Deep
432 Neural Network for Lithium-ion Capacitors[J]. *eTransportation*, 2020, 5:100078.
- 433 [17] Li W., Jiao Z., Du L., et al. An indirect RUL prognosis for lithium-ion battery under vibration stress using
434 Elman neural network[J]. *International Journal of Hydrogen Energy*, 2019, 44(23): 12270-12276.
- 435 [18] Wang S., Yongcun F., Siyu J., Paul T., Carlos F. Improved anti-noise adaptive long short-term memory neural
436 network modeling for the robust remaining useful life prediction of lithium-ion batteries[J]. *Reliability
437 Engineering and System Safety*, 2023, 230: 108920.
- 438 [19] Li L., Liu Z., Tseng M., et al. Enhancing the Lithium-ion battery life predictability using a hybrid method[J].
439 *Applied soft computing*, 2019, 74:110-121.
- 440 [20] Mengyun Z, Wang S., Yanxin X, et al. Hybrid gray wolf optimization method in support vector regression
441 framework for highly precise prediction of remaining useful life of lithium-ion batteries[J]. *Ionics*, 2023, 29(9).
- 442 [21] Li X., Yuan C., Wang Z. State of health estimation for Li-ion battery via partial incremental capacity analysis
443 based on support vector regression[J]. *Energy (Oxford)*, 2020, 203:117852.
- 444 [22] Feng X., Weng C., He X., et al. Online state-of-Health estimation for li-ion battery using partial charging
445 segment based on support vector machine[J]. *IEEE Transactions on Vehicular Technology*, 2019, 68(9): 8583-
446 8592.
- 447 [23] Zhang S., Zhai B., Guo X., et al. Synchronous estimation of state of health and remaining useful lifetime for
448 lithium-ion battery using the incremental capacity and artificial neural networks[J]. *Journal of Energy Storage*,
449 2019, 26: 100951.1-100951.12.
- 450 [24] Zhao, Qi, Qin, et al. A novel prediction method based on the support vector regression for the remaining useful
451 life of lithium-ion batteries[J]. *Microelectronics & Reliability*, 2018, 85: 99-108.
- 452 [25] Cadini F., Sbarufatti C., Cancelliere F., et al. State-of-life prognosis and diagnosis of Lithium-ion batteries by
453 data-driven particle filters[J]. *Applied Energy*, 2019, 235: 661-672.
- 454 [26] Zhao L., Wang Y., Cheng J. A hybrid method for remaining useful life estimation of Lithium-ion battery with
455 regeneration phenomena[J]. *Applied Sciences*, 2019, 9(9): 1890-1905.
- 456 [27] Li F., Xu J. A new prognostics method for state of health estimation of Lithium-ion batteries based on a mixture
457 of Gaussian process models and particle filter[J]. *Microelectronics Reliability*, 2015, 55(7): 1035-1045.
- 458 [28] Qin T., Zeng S., Guo J. Robust prognostics for state of health estimation of lithium-ion batteries based on an
459 improved PSO-SVR model[J]. *Microelectronics and reliability*, 2015, 55(9-10): 1280-1284.
- 460 [29] Wang Y., Ni Y., Lu S., et al. Remaining useful life prediction of Lithium-ion batteries using support vector
461 regression optimized by artificial bee colony[J]. *IEEE Transactions on Vehicular Technology*, 2019, 68(10):
462 9543-9553.
- 463 [30] Li X., Zhang L., Wang Z., et al. Remaining useful life prediction for lithium-ion batteries based on a hybrid
464 model combining the long short-term memory and Elman neural networks[J]. *Journal of energy storage*,
465 2019,21:510-518.

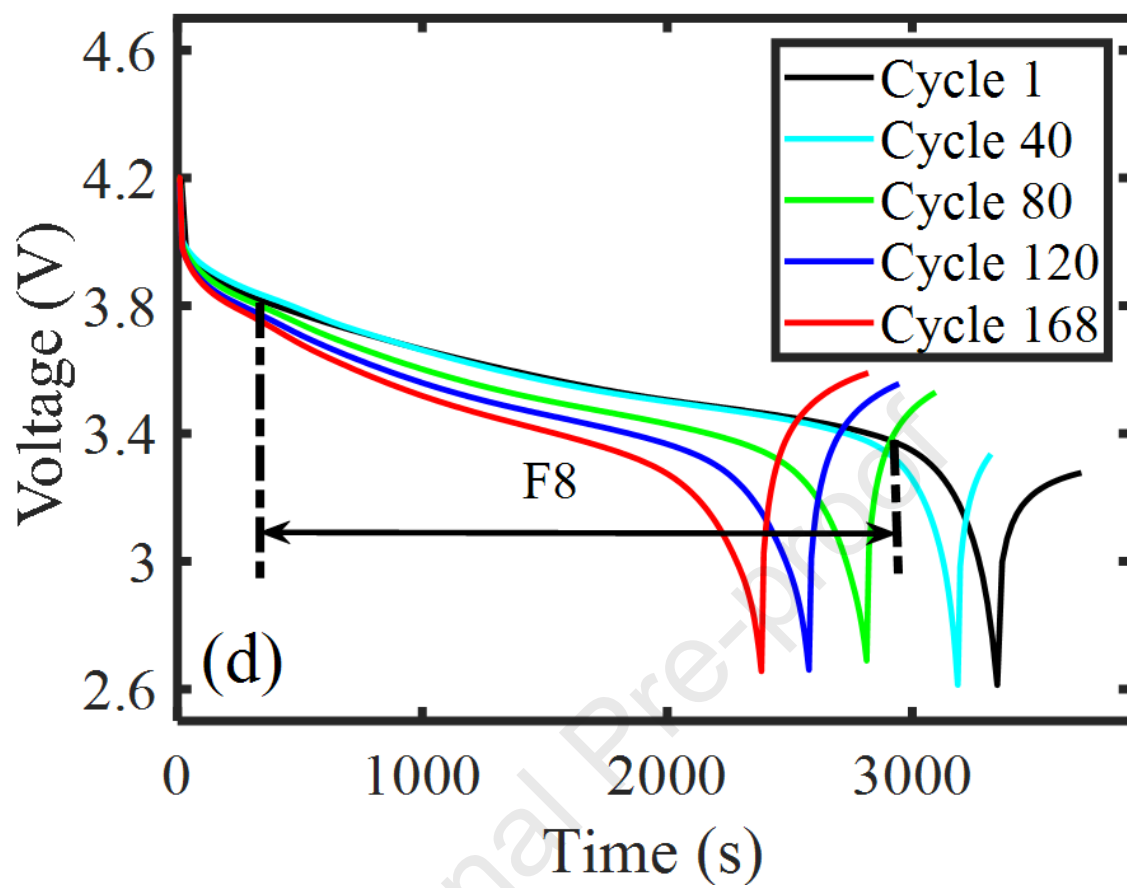
- 466 [31] Jiang Y., Chen L., Zeng W., et al. Adaptive weighted VMD-WPEE method of power-electronic-circuit
467 multiple-parameter-fault diagnosis[J]. IEEE Journal of Emerging and Selected Topics in Power Electronics,
468 2020, (99):3878-3890.
- 469 [32] Shi W., Wen G., Huang X., et al. VMD-scale space based hoyergram and its application in rolling bearing fault
470 diagnosis[J]. Measurement Science and Technology, 2020.
- 471 [33] Xue J., Shen B. A novel swarm intelligence optimization approach: sparrow search algorithm[J]. Systems
472 Science & Control Engineering An Open Access Journal, 2020, 8(1):22-34.
- 473 [34] Qin T., Zeng S., and Guo J. Robust prognostics for state of health estimation of lithium-ion batteries based on
474 an improved PSO-SVR model[J]. Microelectronics Reliability, 2015, 55: 1280 -1284.
- 475 [35] Ma Y., Wu L., Guan Y., et al. The capacity estimation and cycle life prediction of lithium-ion batteries using a
476 new broad extreme learning machine approach[J]. Journal of Power Sources, 2020, 476: 228581.

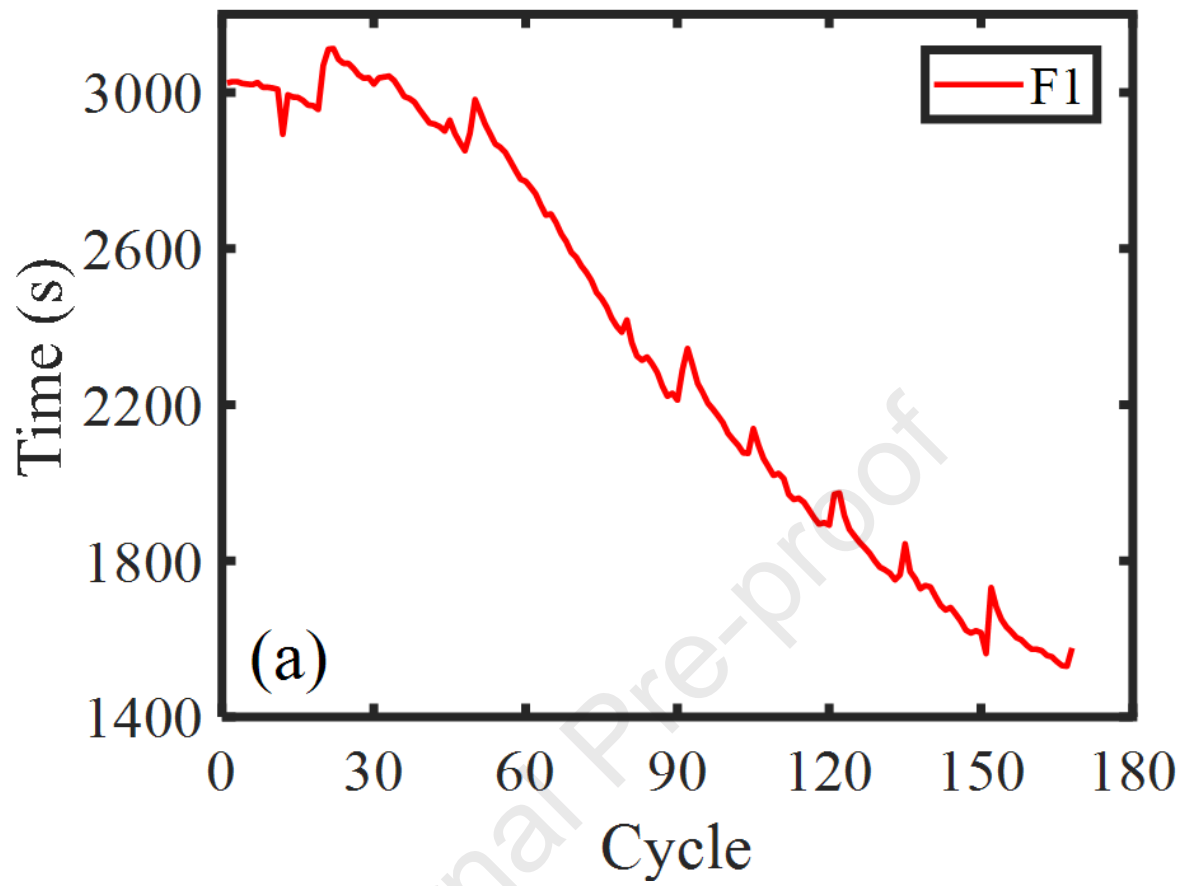


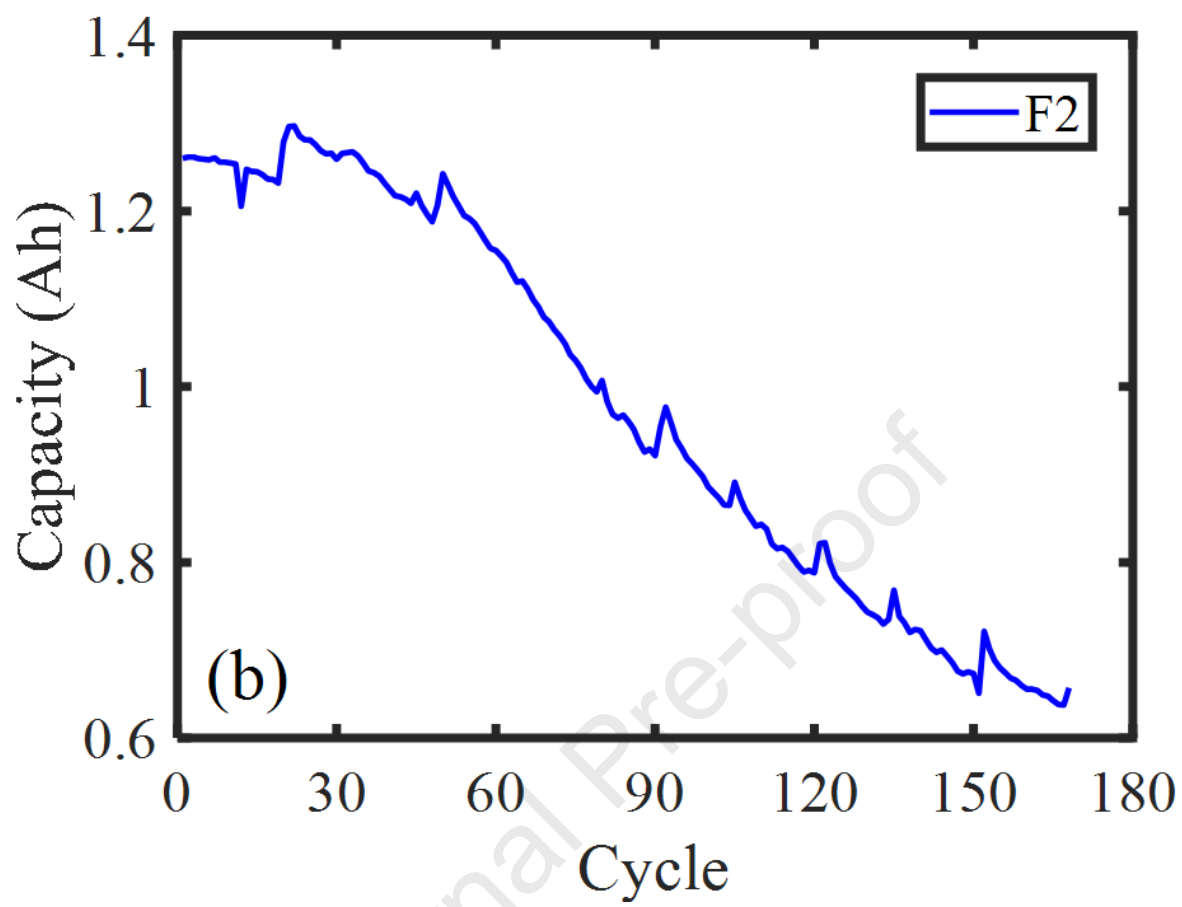


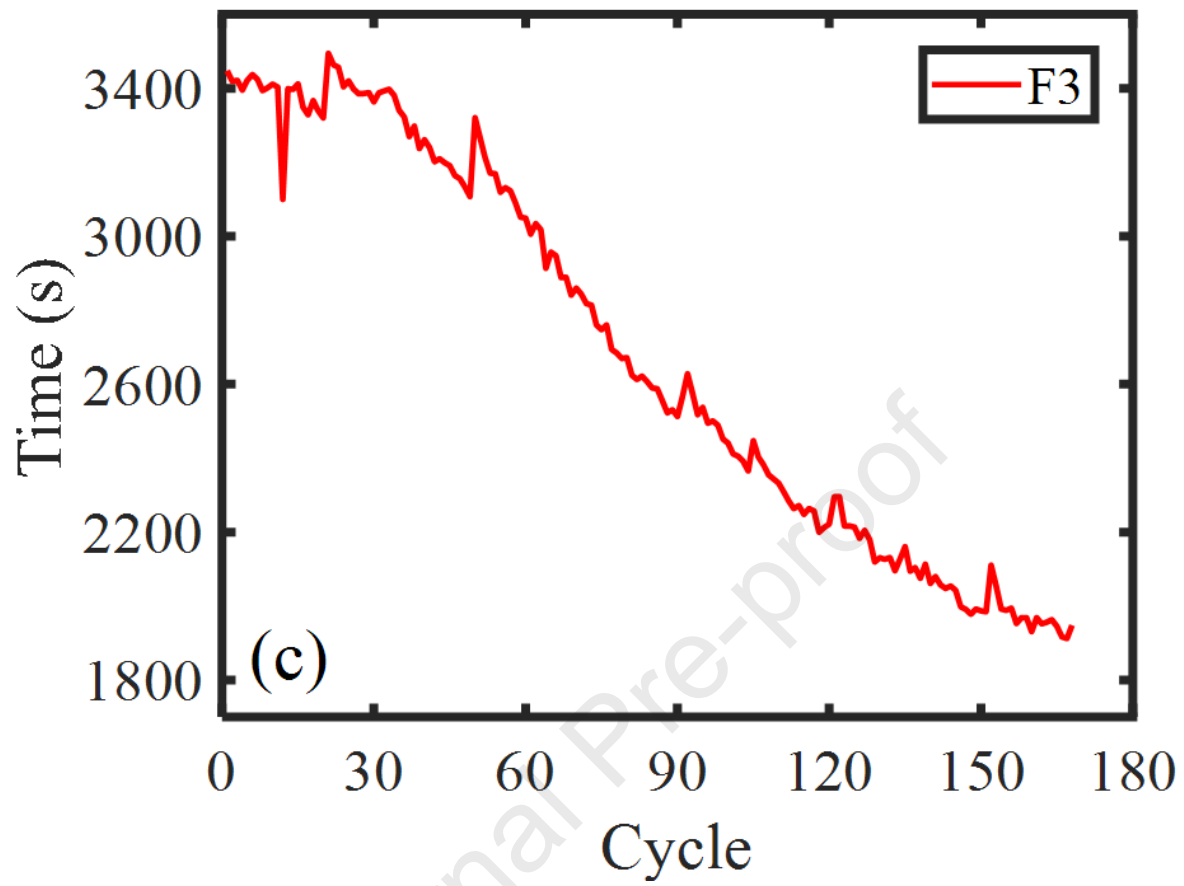


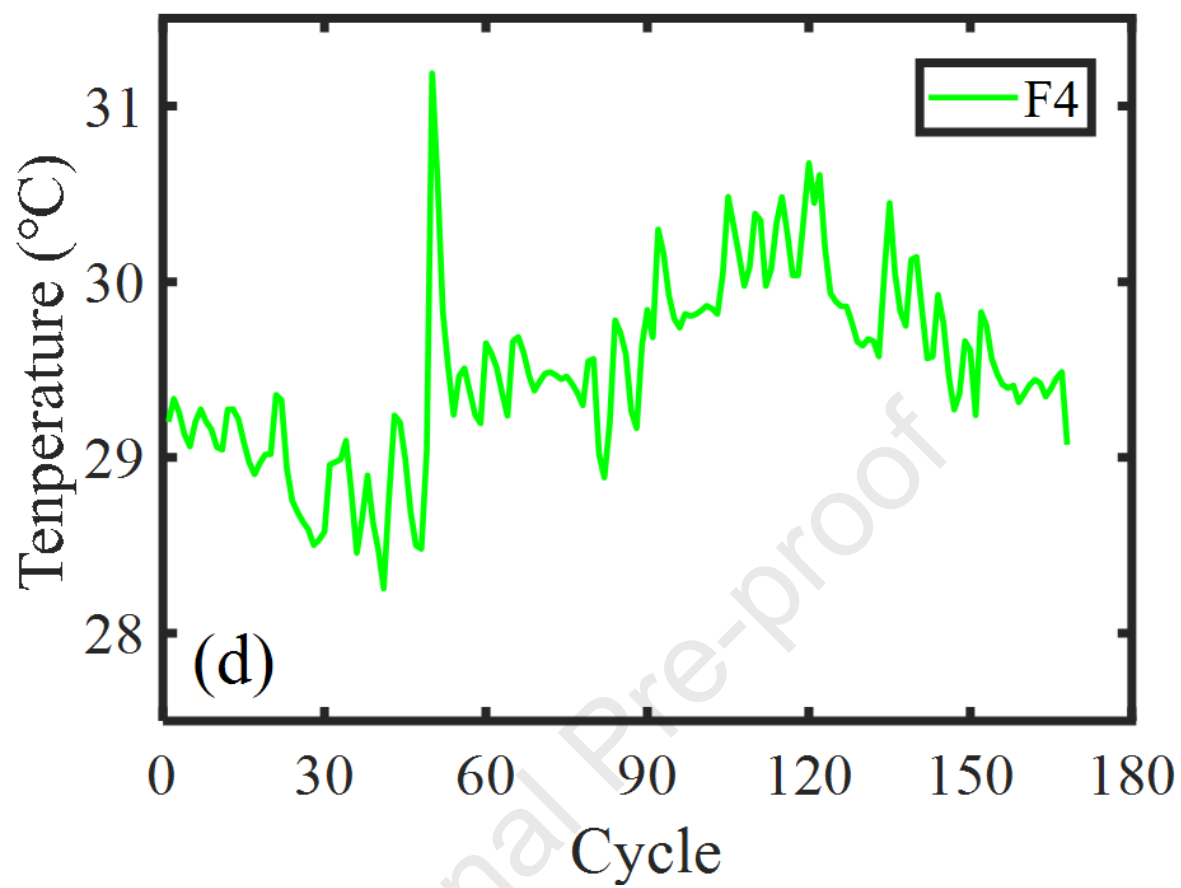


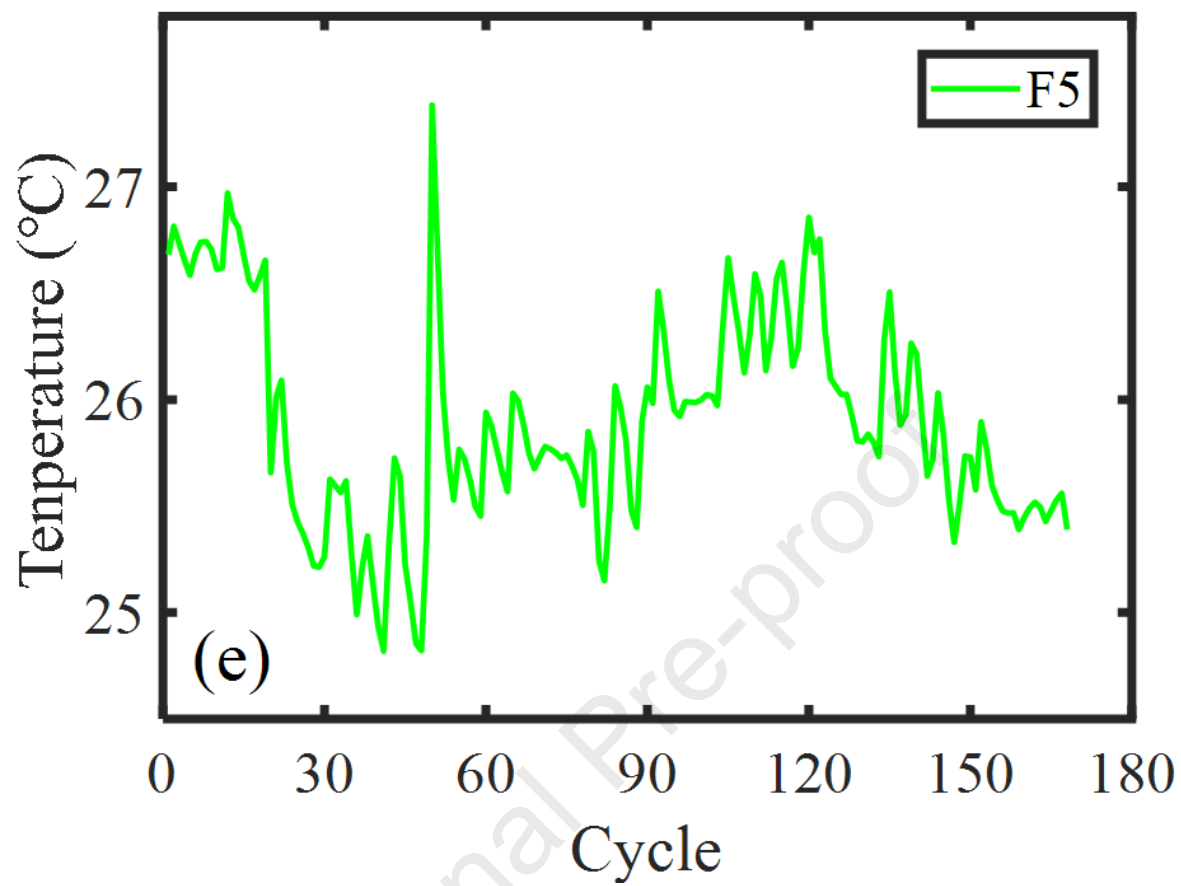


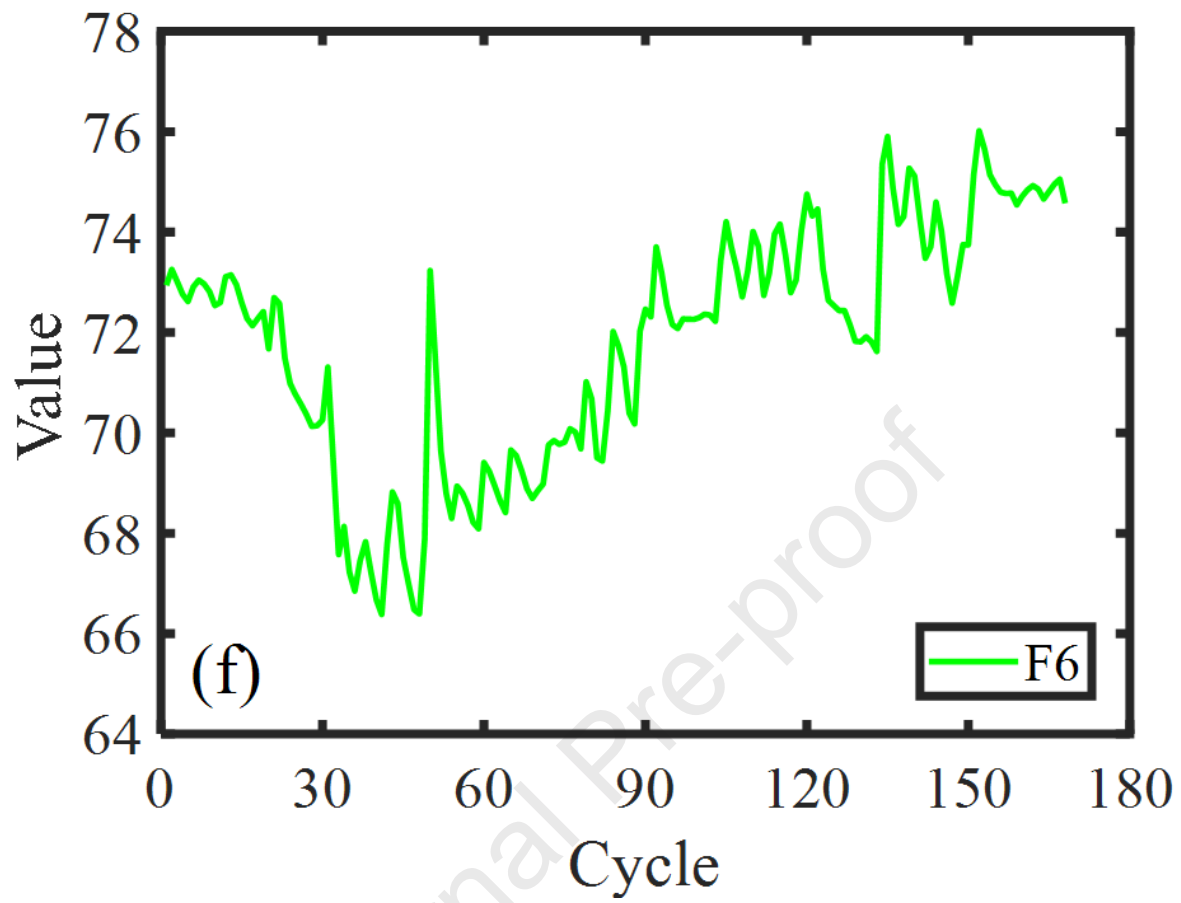


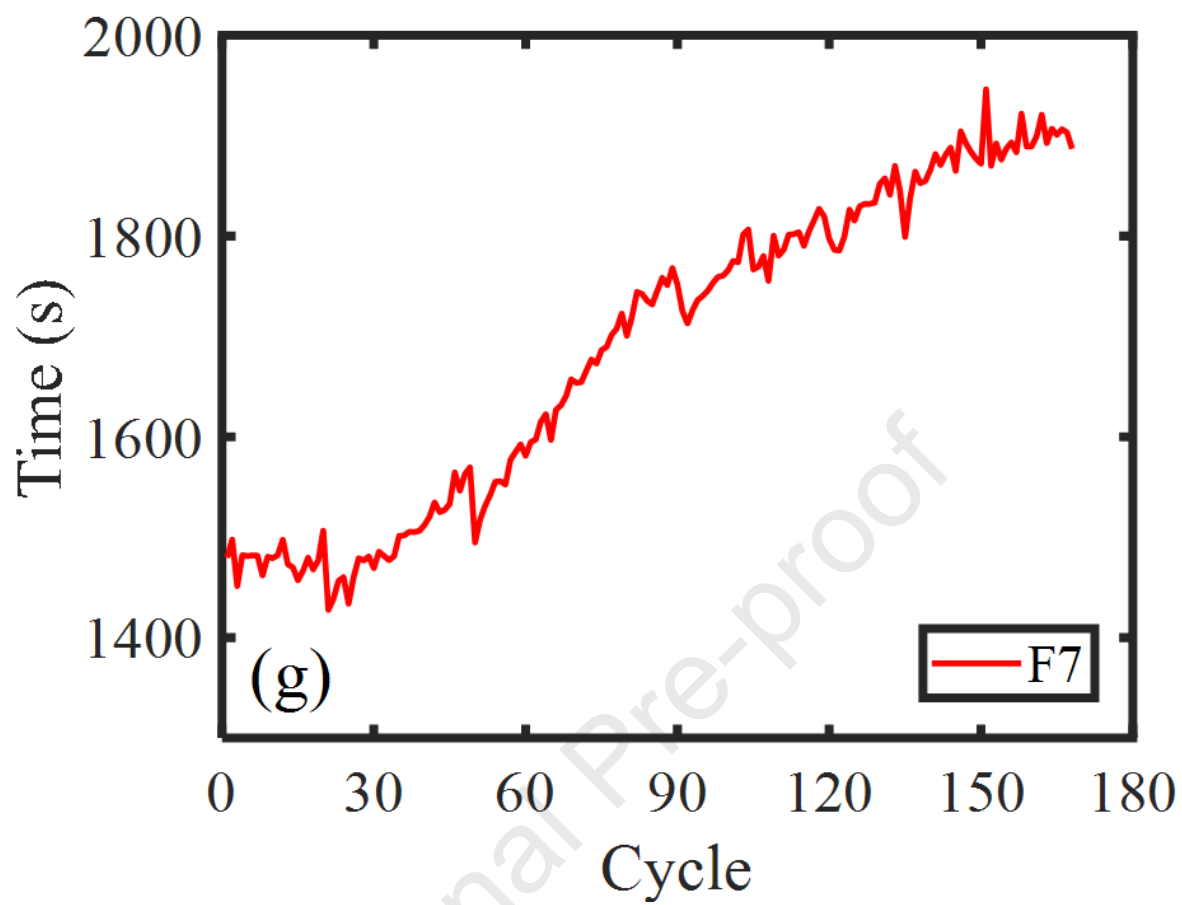


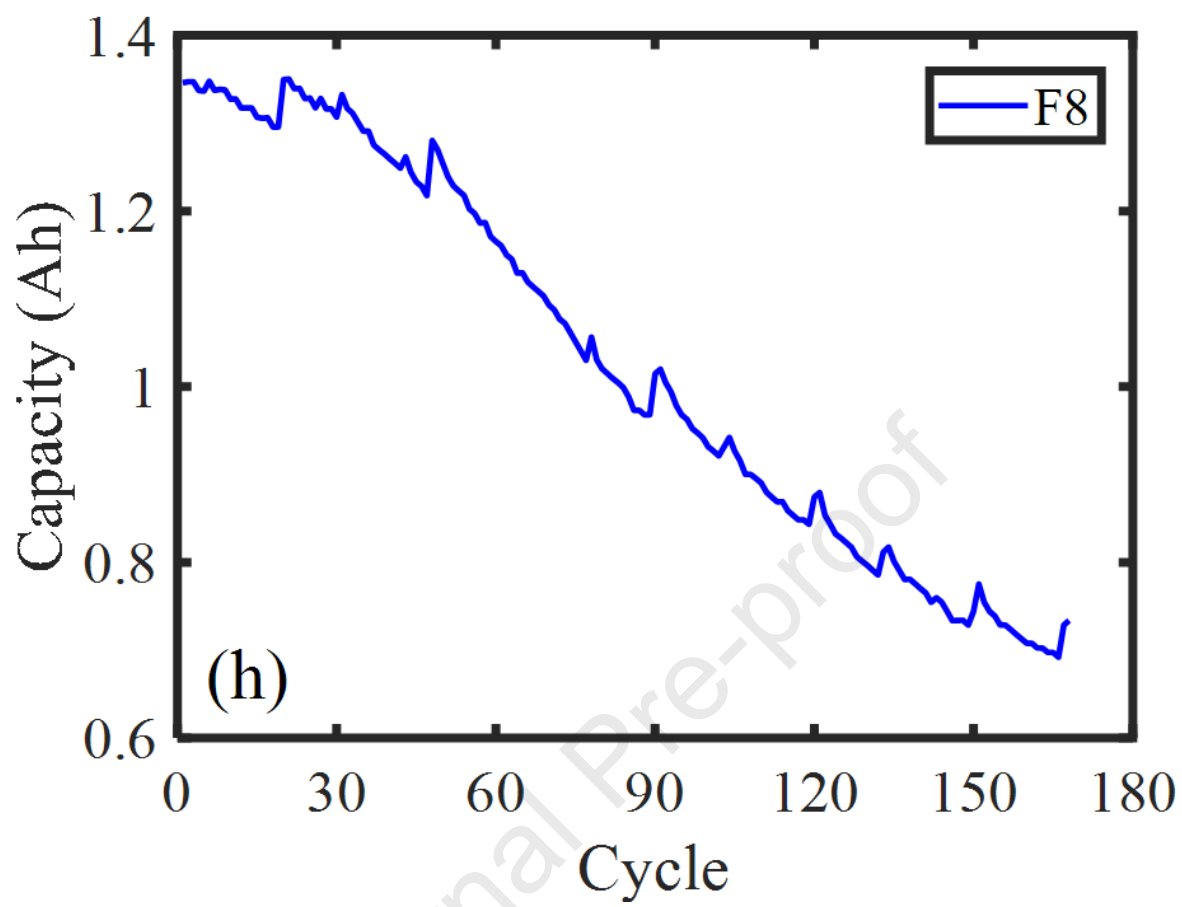


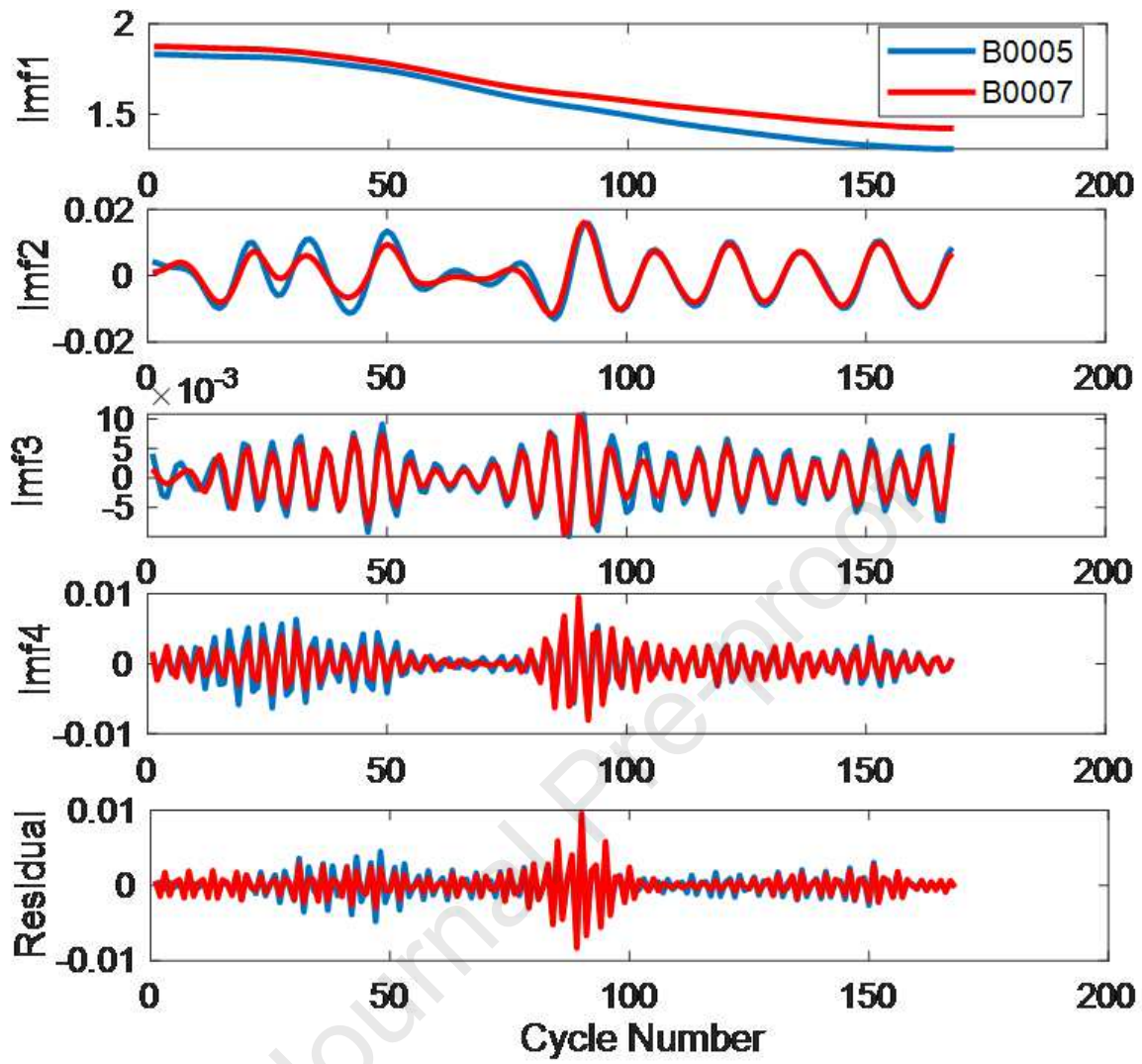


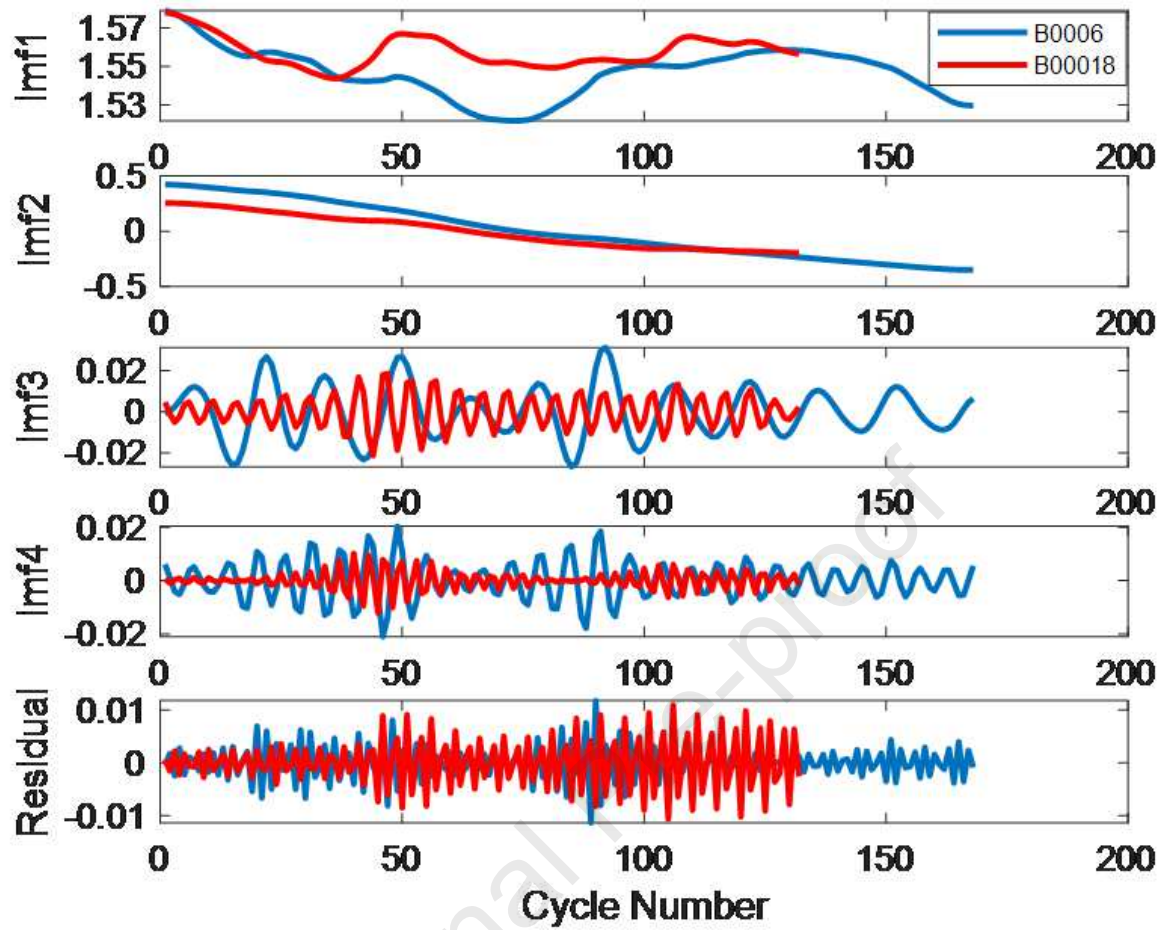


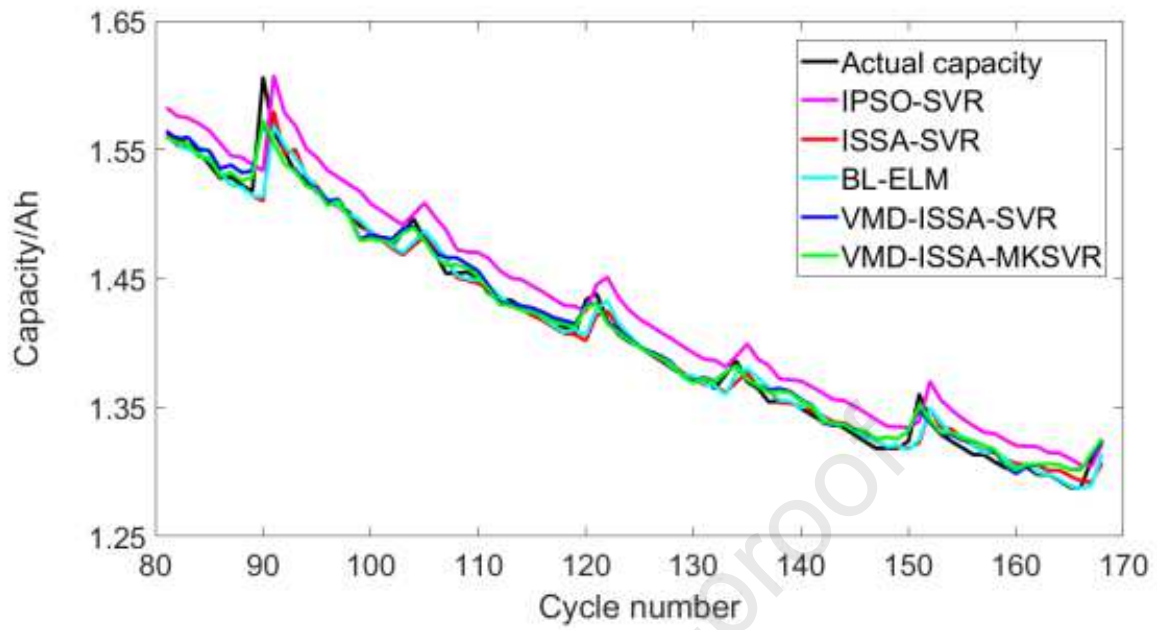


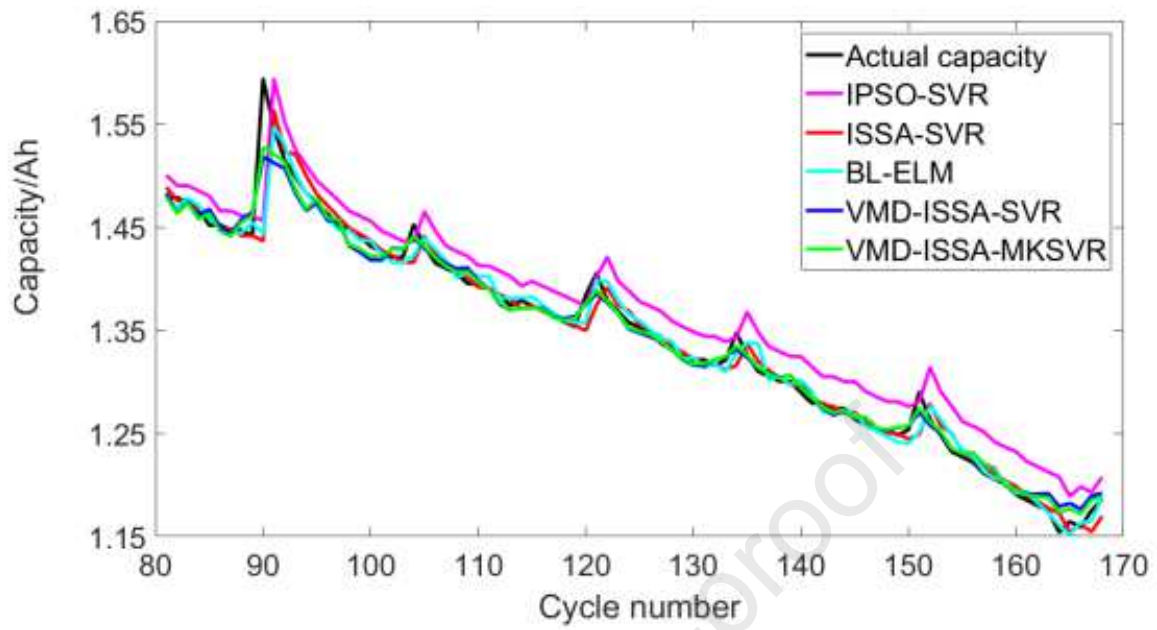


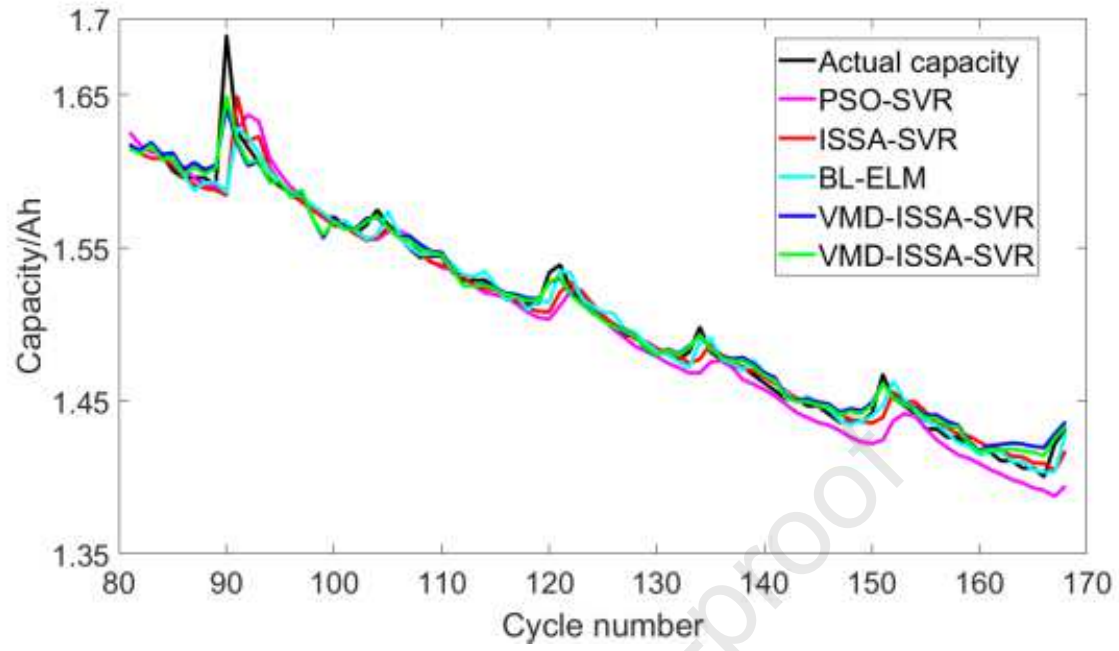


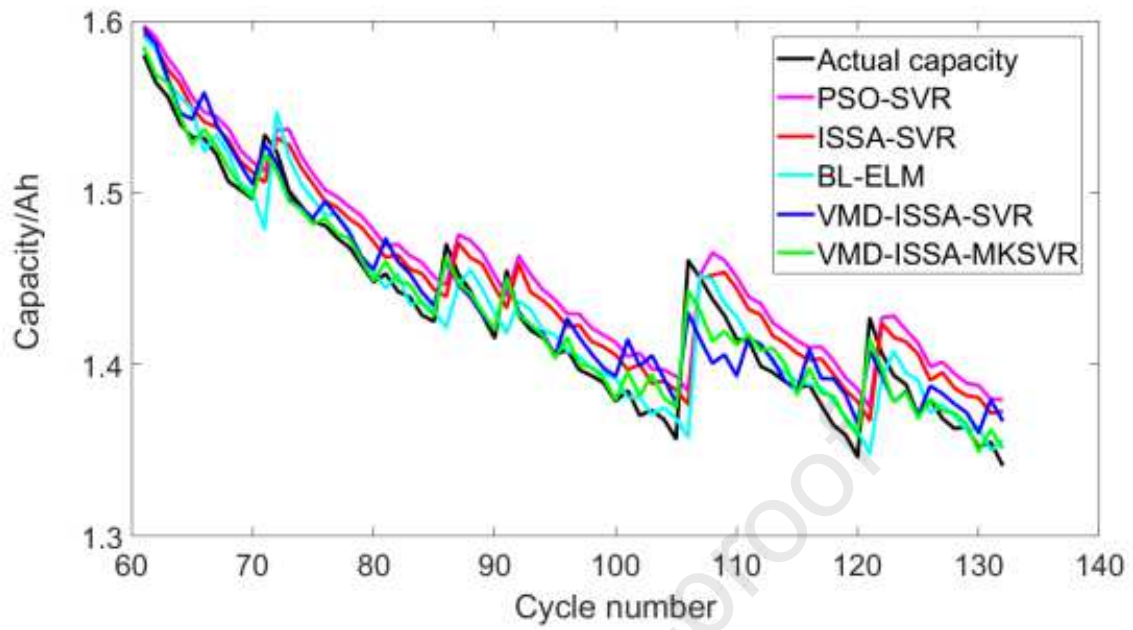


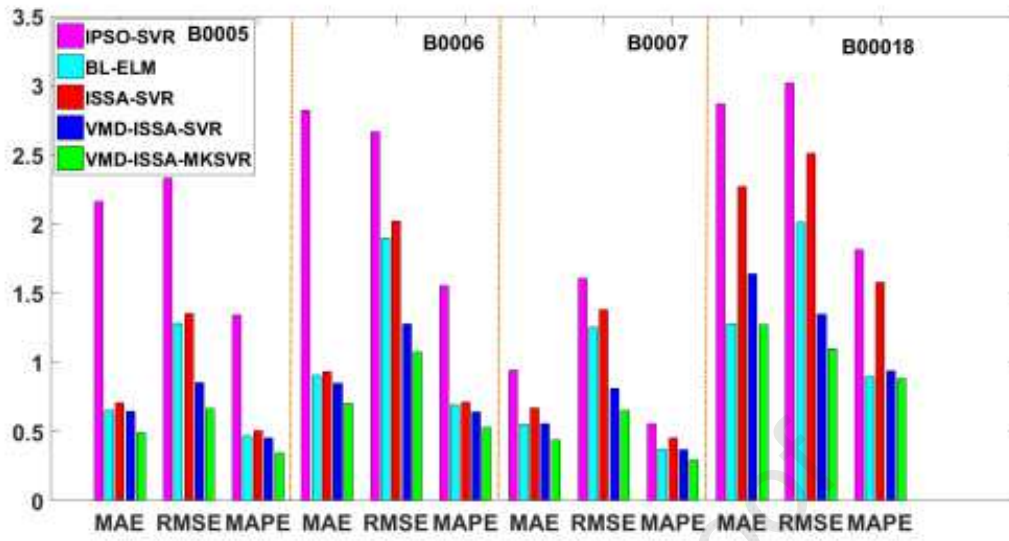


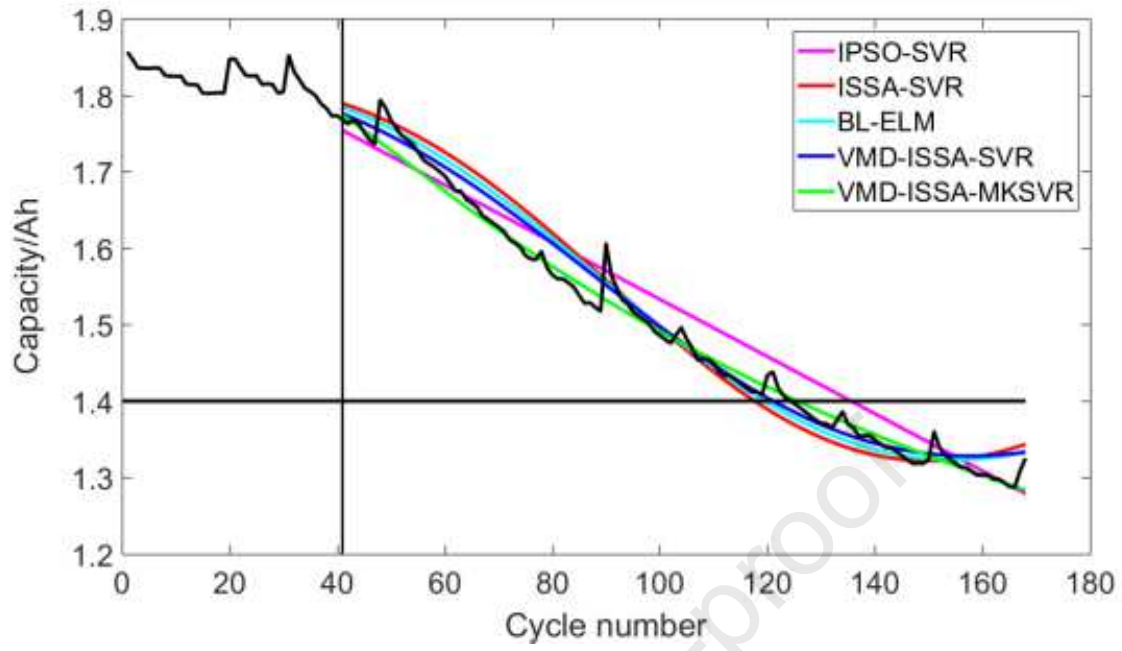


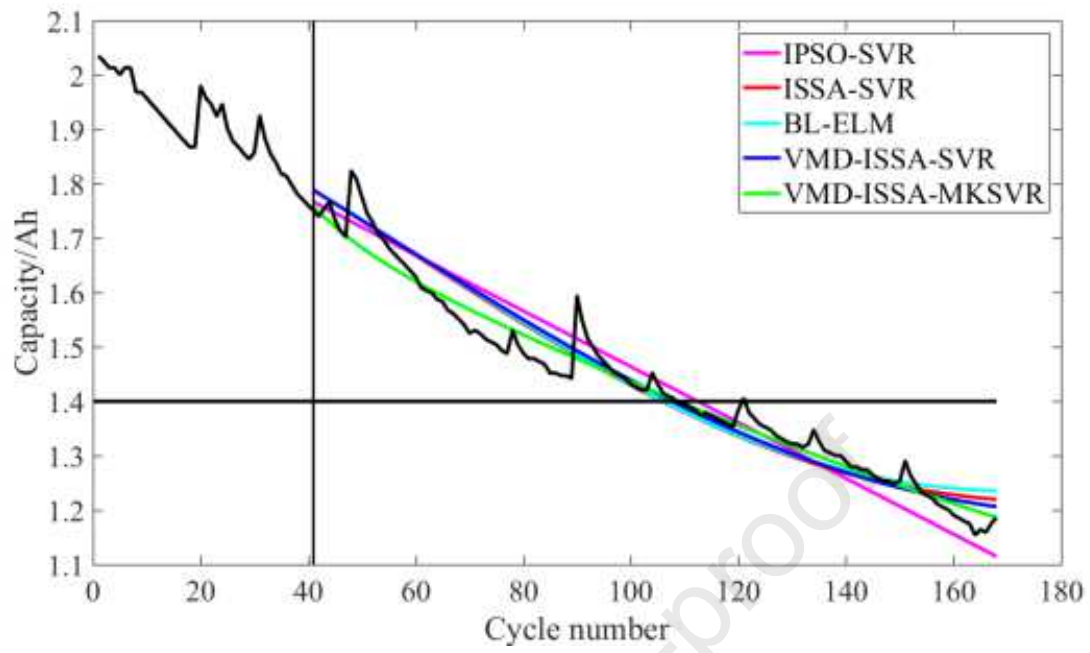


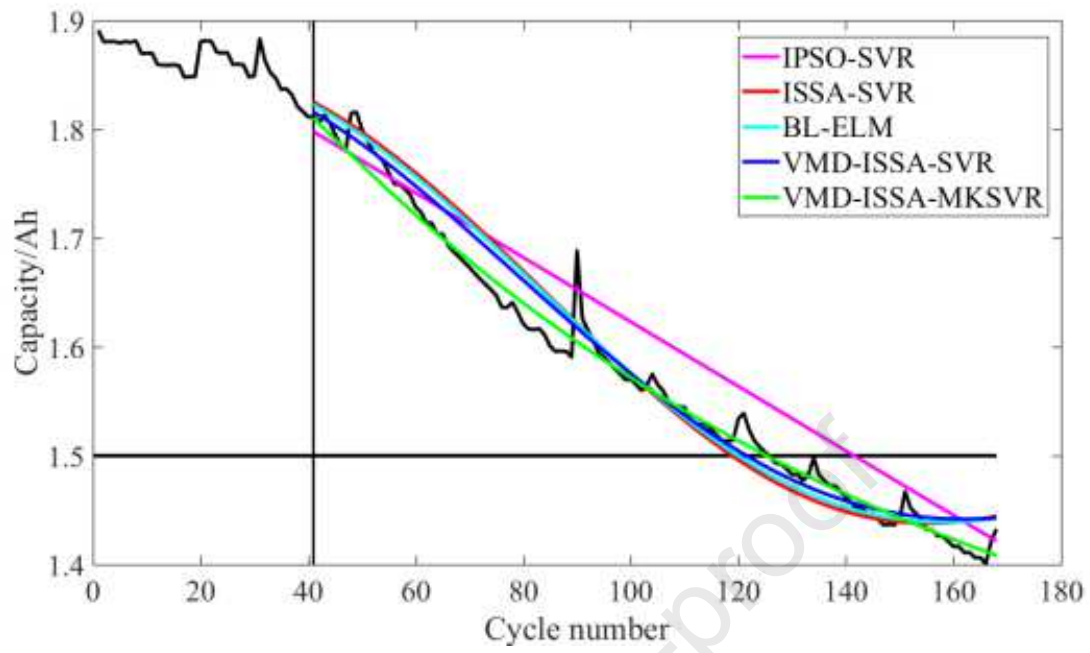


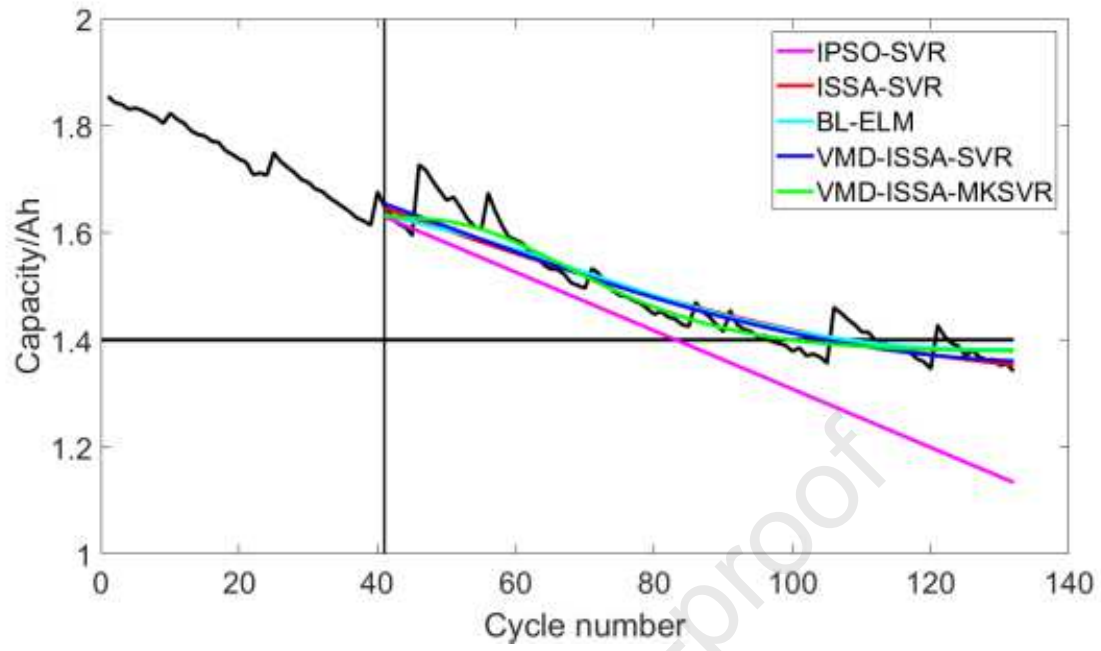












1. A hybrid framework considering feature extraction is proposed to achieve a more accurate and stable prediction performance.
2. The hybrid framework combines variational mode decomposition, the multi-kernel support vector regression model and the improved sparrow search algorithm.
3. Better parameters of the estimation model are obtained by introducing elite chaotic opposition-learning strategy and adaptive weights to optimize the sparrow search algorithm.
4. By feature extraction, the measured data can be directly fed into the life prediction model.

Journal Pre-proof

This manuscript has complied with Elsevier's ethical requirements:(Submission of an article implies that the work described has not been published previously (except in the form of an abstract or as part of a published lecture or academic thesis), that it is not under consideration for publication elsewhere, that its publication is approved by all authors and tacitly or explicitly by the responsible authorities where the work was carried out. Submission also implies that, if accepted, it will not be published elsewhere in the same form, in English or in any other language, without the written consent of the Publisher.)

All authors disclosed no relevant relationships

Journal Pre-proof

Declaration of interests

The authors declare that they have no known competing financial interests or personal relationships that could have appeared to influence the work reported in this paper.

The authors declare the following financial interests/personal relationships which may be considered as potential competing interests:

Journal Pre-proof